Article

Cell

Type VI Secretion System Substrates Are Transferred and Reused among Sister Cells

Graphical Abstract

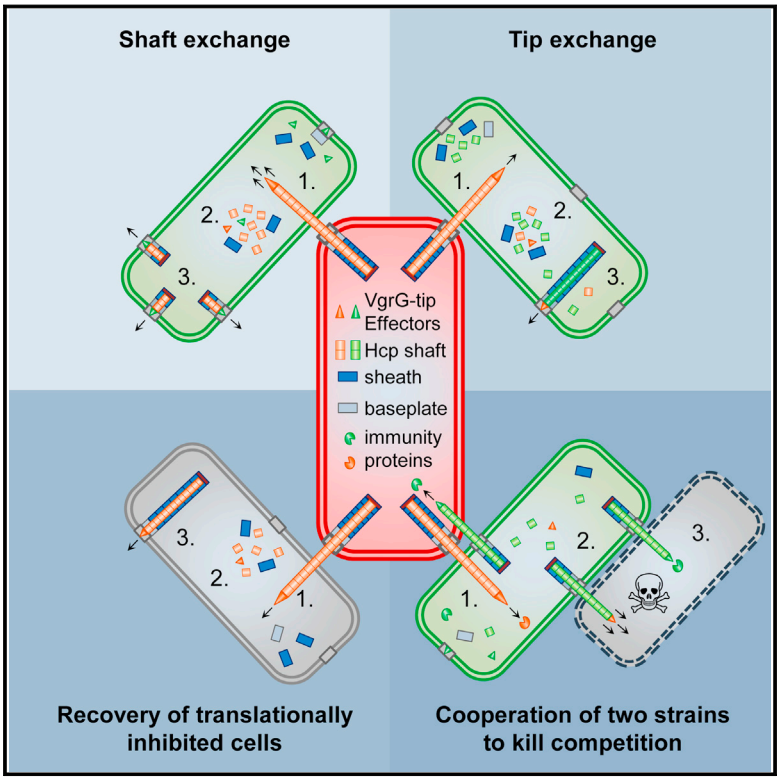

Authors

Andrea Vettiger, Marek Basler

Correspondence

marek.basler@unibas.ch

In Brief

Bacteria use proteinaceous spear guns to attack one another and can reuse the components that entered their cytosol in this manner.

Highlights

- Proteins secreted by T6SS are exchanged among cells and reused for T6SS assembly
- Amount of VgrG limits number of T6SS assemblies and Hcp limits the sheath length
- T6SS-dependent exchange of secreted proteins increases chances to kill competition
- Efficiency of protein exchange depends on precise aiming of T6SS

Vettiger & Basler, 2016, Cell *167*, 99–110
September 22, 2016
http://dx.doi.org/10.1016/j.cell.2016.08.023

CellPress

Article

Cell

Type VI Secretion System Substrates Are Transferred and Reused among Sister Cells

Andrea Vettiger[1] and Marek Basler[1,2,*]
[1]Focal Area Infection Biology, Biozentrum, University of Basel, Basel, Switzerland
[2]Lead Contact
*Correspondence: marek.basler@unibas.ch
http://dx.doi.org/10.1016/j.cell.2016.08.023

SUMMARY

Bacterial type VI secretion system (T6SS) is a nanomachine that works similarly to a speargun. Rapid contraction of a sling (sheath) drives a long shaft (Hcp) with a sharp tip and associated effectors through the target cell membrane. We show that the amount and composition of the tip regulates initiation of full-length sheath assembly and low amount of available Hcp decreases sheath length. Importantly, we show that both tip and Hcp are exchanged by T6SS among by-standing cells within minutes of initial cell-cell contact. The translocated proteins are reused for new T6SS assemblies suggesting that tip and Hcp reach the cytosol of target cells. The efficiency of protein translocation depends on precise aiming of T6SS at the target cells. This interbacterial protein complementation can support T6SS activity in sister cells with blocked protein synthesis and also allows cooperation between strains to increase their potential to kill competition.

INTRODUCTION

Membranes play an important role in protecting cellular contents from the outside environment. However, sophisticated mechanisms evolved to overcome the protection. One such mechanism is mechanical breach of the membrane by puncturing using a sharp tip. This principle is used by many systems related to contractile phage tails such as bacterial type VI secretion system (T6SS) or R-type pyocins (Cianfanelli et al., 2016; Leiman and Shneider, 2012; Zoued et al., 2014). T6SS was identified in many gram-negative bacteria and its expression as well as subcellular localization is regulated by several different mechanisms (Ho et al., 2014; Silverman et al., 2012). The different T6SSs secrete wide variety of effector molecules into both bacterial and eukaryotic targets making T6SS essential for bacterial competition and pathogenesis (Alcoforado Diniz et al., 2015; Durand et al., 2014; French et al., 2011; Hachani et al., 2016; Hood et al., 2010; Ma et al., 2014; MacIntyre et al., 2010; Pukatzki et al., 2006; Russell et al., 2014). An explanation for such a remarkable flexibility of T6SS could be its unique mode of action, which resembles a spear gun. T6SS is composed of a shaft with a sharp tip carrying a payload, a sling and a baseplate attached to the bacterial cell envelope. The shaft is a hollow tube built from rings of Hcp hexamers and is surrounded by a contractile sling called sheath composed of six helical strands of VipA/VipB (or TssB/TssC) heterodimers (Bönemann et al., 2009; Brunet et al., 2014; Kudryashev et al., 2015; Mougous et al., 2006). The tube begins with a tip complex composed of VgrG trimer, PAAR protein, and various effectors (Dong et al., 2013; Flaugnatti et al., 2016; Hachani et al., 2014; Pukatzki et al., 2007; Shneider et al., 2013; Unterweger et al., 2014). The tube-sheath complex assembles in the cytoplasm from a cell envelope-associated baseplate and can be as long as the width of the cell (Basler et al., 2012; Brunet et al., 2015; Durand et al., 2015; Gerc et al., 2015; Zoued et al., 2016). Upon an unknown signal from the baseplate, the sheath rapidly contracts to about half of its length and ejects the tube with the associated effectors out of the cell and across a target cell membrane (Basler et al., 2012). The contracted sheath is specifically recognized by a T6SS-associated ATPase, ClpV, which unfolds VipB to allow for new sheath assembly (Basler and Mekalanos, 2012; Bönemann et al., 2009; Kapitein et al., 2013; Pietrosiuk et al., 2011). VipA and ClpV fluorescent protein fusions were shown to be fully functional and their dynamic localization correlates with T6SS activity (Basler and Mekalanos, 2012; Basler et al., 2012; Brunet et al., 2013; Clemens et al., 2015; Gerc et al., 2015; Kapitein et al., 2013; Kudryashev et al., 2015).

T6SS activity is regulated on transcriptional level in a response to wide variety of signals (Miyata et al., 2013; Silverman et al., 2012). For example, certain *Vibrio cholerae* strains grown to a high cell density in presence of chitin co-regulate DNA uptake machinery and T6SS activity to acquire new genes (Borgeaud et al., 2015). Assembly of H1-T6SS of *Pseudomonas aeruginosa* is localized subcellularly with a high precision to direct the secretion toward the target cells for their efficient killing (Basler et al., 2013; Ho et al., 2013; LeRoux et al., 2012). Additionally, in *V. cholerae* secreted proteins VgrG2 and Hcp as well as VasX and VgrG3 effectors were shown to be required for proper T6SS assembly (Dong et al., 2013; Kapitein et al., 2013; Pukatzki et al., 2006, 2007). Many anti-bacterial effectors have periplasmic targets, such as peptidoglycan or membrane (Russell et al., 2014), however, some others, such as DNases, clearly need to reach the bacterial cytosol (Koskiniemi et al., 2013; Ma et al., 2014). It is unclear if T6SS is capable to breach both membranes and peptidoglycan at the same time or if cytosolic effectors use separate mechanism to translocate from periplasm to cytosol similarly to the recently described effector of *P. aeruginosa*, which requires EF-Tu to cross inner membrane (Whitney et al., 2015).

Here, we show that Hcp, VgrG2, and T6SS effectors of *V. cholerae* are exchanged between neighboring cells and can be efficiently reused for a new T6SS assembly. We further show that availability of tip complex limits number of T6SS assemblies per cell and Hcp concentration regulates length of T6SS sheaths. Our data also suggest that both Hcp tube and tip complex are delivered to the cytosol of a target cell and both are disassembled to be reused for a new functional T6SS assembly. We show that efficiency of this interbacterial protein complementation depends on accurate aiming of T6SS activity and may under certain conditions help cells to fight competition.

RESULTS

Hcp and VgrG2 Are Exchanged between Cells and Reused for a New T6SS Assembly

We designed our experiments to test if VgrG and Hcp proteins are exchanged between bacteria based on two previous observations: (1) T6SS sheath assembles into a long dynamic structure, which is a hallmark of a functional T6SS, and (2) some T6SS substrates are necessary for T6SS function. Here, we observed that *V. cholerae* cells with a fully functional T6SS contained on average 3.2 VipA-msfGFP sheath structures per cell at any given time and assembled on average 5.6 structures per 5 min. In contrast, no sheaths were assembled in cells lacking *vgrG2*, *hcp1/hcp2*, or *vgrG2/hcp1/hcp2*, respectively in more than 20,000 cells (Figures 1A and S1; Movie S1; for a complete strain list, see Table S1). Importantly, these cells were also unable to kill *Escherichia coli* prey cells or secrete Hcp (Figures S2A–S2C). We mixed these cells deficient in sheath assembly (recipient) with T6SS$^+$ (donor) cells at a ratio of 1:4 and monitored localization of VipA-msfGFP in the recipient cells by fluorescence microscopy (Figure 1B). Surprisingly, the sheath assembly was restored in the recipient strain as more than 1 in 20 cells assembled at least one sheath structure within 5 min of imaging (Figures 1C–1E and 1H; Movies S2, S3, and S4). This was fully dependent on a functional T6SS in the donor cells because no sheath assembly was detected in the recipient cells mixed with donor cells lacking *vipB* (Figure 1F). Importantly, T6SS$^+$ donor cells failed to rescue sheath assembly in recipient cells lacking non-secreted VipB sheath component (Figure 1G). The recipient cells were also unable to directly uptake VgrG and Hcp proteins from the environment as no sheath assembly was detected upon incubation with 10-fold concentrated supernatant of wild-type cells containing both VgrG2 and Hcp (Figure S3). Furthermore, distance measurement between donor and recipient cells showed that sheath assembly was ten times more frequent in the recipient cells that were in a direct contact to T6SS$^+$ donor cells than in those that were further away (Figure 1I) and reached ~2% of the frequency of sheath assembly in the wild-type cells (Figures 1H and 1I).

To test if DNA, RNA, or protein transfer was responsible for restoring sheath assembly, we inhibited protein synthesis in the recipient cells lacking *vgrG2* by 30 min pre-incubation in the presence of chloramphenicol. Such treatment failed to inhibit sheath assembly in the recipient cells mixed with wild-type cells (Figures S4B and S4C). In contrast, chloramphenicol treatment fully blocked sheath assembly in the recipient cells after expression of *vgrG2* was induced from pBAD24 plasmid (Figure S4A). Taken together, this indicates that secreted proteins such as VgrG2 and Hcp can be exchanged between cells by T6SS-dependent translocation and that the exchanged proteins can be reused for a new T6SS assembly.

Availability of VgrG2 Limits the Number of Sheath Assemblies and Hcp Limits the Sheath Length

A detailed comparison of length and number of T6SS sheaths assembled in the recipient cells after complementation of VgrG2 or Hcp revealed unexpected differences (Figures 1C and 1E). In case of VgrG2, the sheath structures that formed in the recipient cells were stretching from one side of a cell to another and were on average 0.60 μm long. These structures were therefore indistinguishable from structures assembled in the wild-type cells that were on average 0.62 μm long (Figure 2A). However, mostly only a single structure assembled in the recipient cell during 5 min (Figure 2B). In case of Hcp complementation, the average length of assembled sheath structures was 0.25 μm, which is less than half of the length in wild-type cells. Because this length is close to the diffraction limit of the optical microscope, it is likely that many of these sheath structures were in fact even shorter. The number of structures assembled during Hcp complementation was on average 3.1 and thus significantly higher than in case of VgrG2 complementation and similar to number of assemblies in wild-type cells (Figures 2A and 2B). During simultaneous complementation of VgrG2 and Hcp, 1.7 structures per cells assembled on average and the average sheath length was 0.36 μm (Figures 1D, 2A, and 2B).

Interestingly, the first sheath assembly in *vgrG2*-negative recipient cells was detected as quickly as 2 min after mixing with T6SS$^+$ donor cells (Figure 2C). This is remarkable considering that at these imaging conditions the wild-type cells contract T6SS sheath on average only approximately once per minute as estimated from ClpV-mCherry2 localization (Movies S2, S3, and S4). Because close contact is necessary for the protein transfer, a recipient cell can be within a reach of only limited number of cells and thus could receive only few VgrG complexes in 2 min. On the other hand, sheath assembly during Hcp complementation was first detected after 28 min of incubation (Figure 2C). This suggests that even though protein transfer starts immediately after the cells are in close contact, the concentration of Hcp in the cytosol has to reach certain threshold to initiate sheath assembly or be sufficient for assembly of sheaths detectable by fluorescence microscopy.

To test how amount of available VgrG2 and Hcp influences T6SS assembly, we expressed Hcp or VgrG2 from an inducible pBAD plasmid in cells lacking *hcp1/hcp2* or *vgrG2*, respectively. The protein expression was induced at the same time as imaging was initiated by spotting the cells on an agarose pad containing 0.1% L-arabinose. Shortly after induction of VgrG2, only few full-length sheath assemblies were detected in the cells, however, after 40 min of induction, the number of full-length structures reached wild-type levels (Figure 2D; Movie S5). On the other hand, short induction of Hcp resulted in assembly of multiple short sheath structures and longer induction only increased the sheath length without further increasing the number of structures per cell (Figure 2E; Movie S5). Small amounts of Hcp or VgrG2 protein, barely detectable using western blot analysis, are

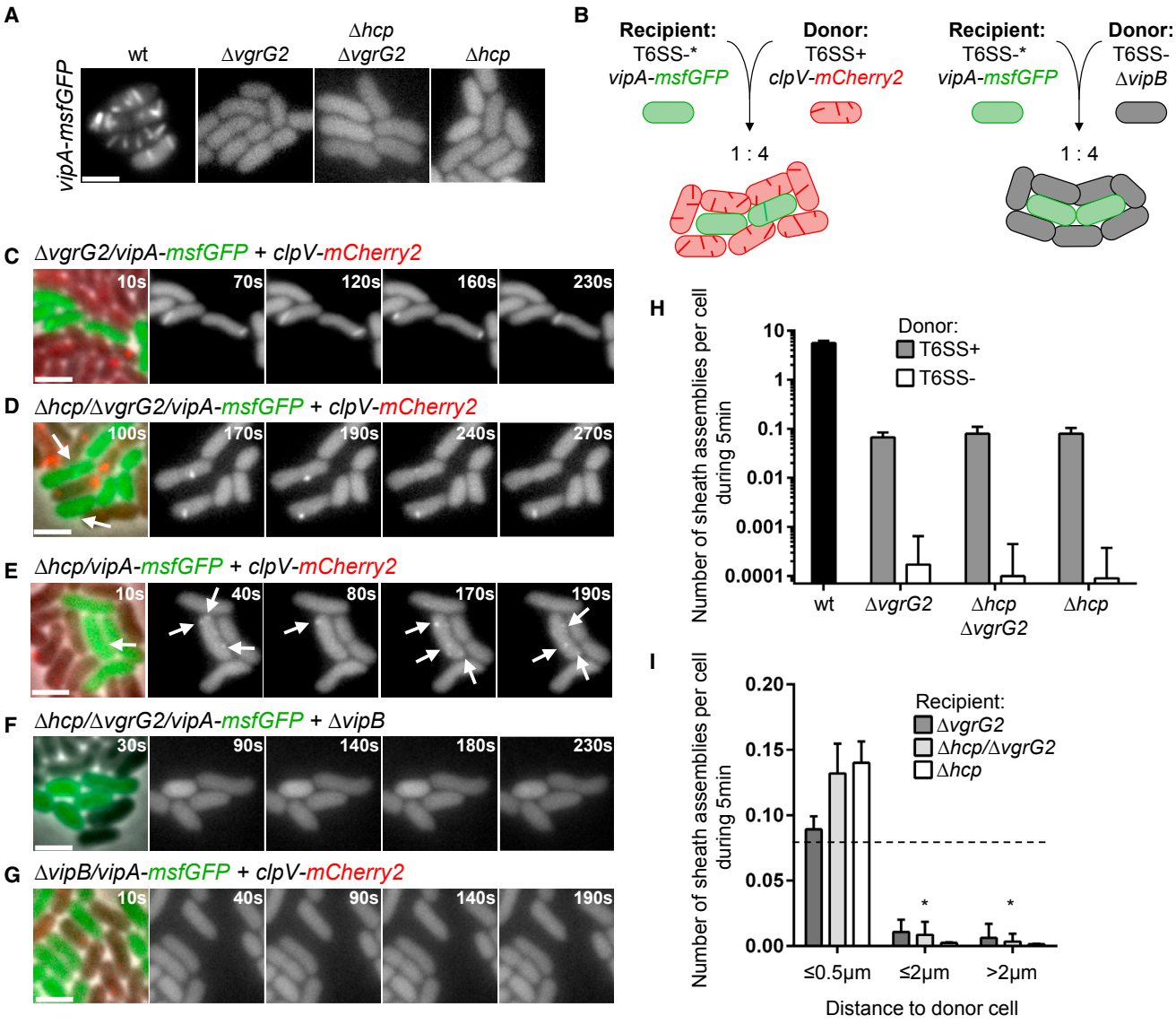

Figure 1. T6SS Activity Can Be Partially Restored in T6SS⁻ Cells by Interbacterial Protein Complementation from T6SS⁺ Cells

(A) VipA-msfGFP localization (sheath assembly) was monitored in at least 20,000 cells of the indicated strains over 5 min. Representative images of GFP fluorescence channel are shown. Additional images with a bigger field of view can be found in Figure S1 and Movie S1.

(B) The interbacterial protein complementation assay: Bacterial mixtures were spotted on a 1% LB-agarose pad and imaged during 2 hr at 25°C. Asterisk marks T6SS⁻ strains with deleted secreted components.

(C–G) Indicated recipient strains (green, T6SS⁻) were mixed with donor strains (unlabeled, T6SS⁻; red, T6SS⁺) and monitored for sheath assembly for 2 hr. Depicted are individual frames of a 5-min time-lapse movie. The first frame shows all cells and is a merge of phase contrast, GFP, and mCherry2 fluorescence channels (where applicable). The next four frames only show GFP fluorescence channel to clearly visualize sheath dynamics. Arrows highlight dynamics of short VipA-msfGFP structures. See Movies S2, S3, and S4 for complete time-lapse movies.

(H) Sheath assembly was monitored in the indicated strains for 5 min after 30 min co-incubation with either T6SS⁺ or T6SS⁻ donor cells. Total number of sheath assemblies was counted for at least 5,000 GFP⁺ cells for each combination of indicated strains. Black bar depicts T6SS assembly rate in wild-type.

(I) For a total number of 20,915 GFP⁺ cells distance to the next donor cell was analyzed. GFP⁺ cells were grouped into three indicated categories based on the distance. Sheath assembly was monitored in the indicated strains for 5 min. Dashed line represents mean protein complementation frequency for total cell number as depicted in Figure 1H. *$p < 0.0001$ as compared to ≤ 0.5 μm; two-way ANOVA with multiple comparison and Tuckey post hoc correction; number of cells per category: ≤ 0.5 μm, N = 14,388; ≤ 2 μm, N = 4,356; >2 μm, N = 3,639.

All data represented in this figure are shown as mean ± SD were acquired from six independent biological replicates. Scale bar, 2 μm on all images.

See also Figures S2, S3, and S4.

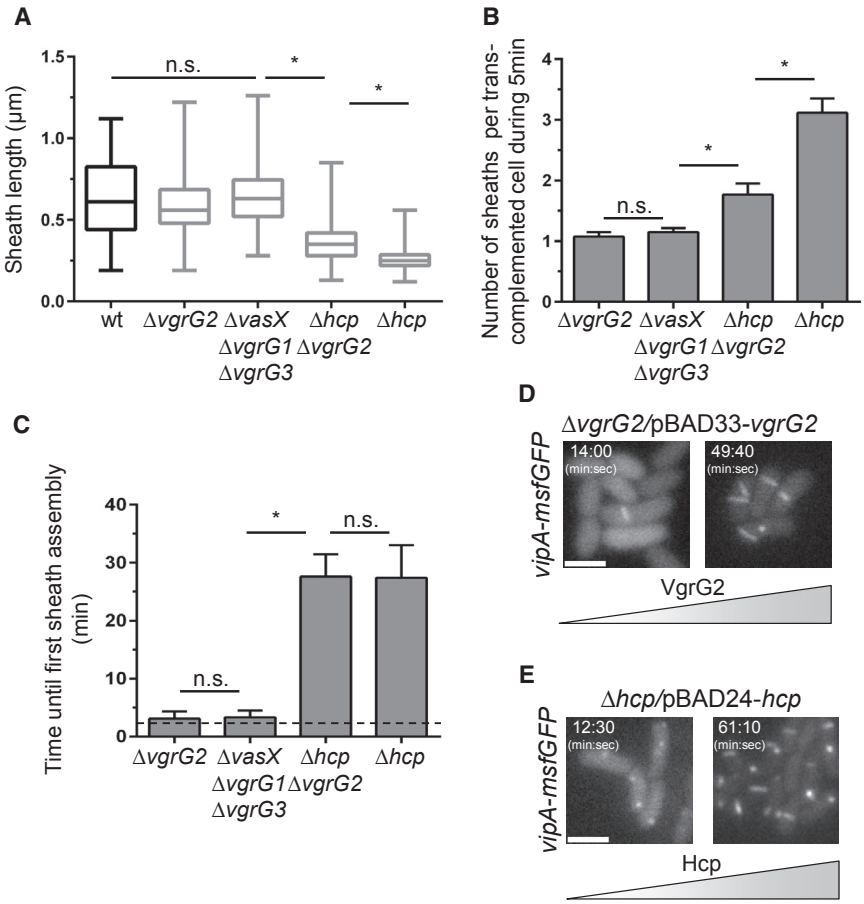

Figure 2. Tip Protein Concentration Dictates Number of Sheaths per Cell, whereas Hcp Determines Sheath Length

(A) Sheath length was measured from 100 fully extended structures in wild-type *vipA-msfGFP* strain (black graph) and in the indicated recipient strains (all *vipA-msfGFP* background) mixed with T6SS$^+$ donor strain (protein complementation, gray graphs). Depicted are whiskers plots with minima and maxima; 75% of all data points lay within the box, horizontal line represents the median.

(B) Number of sheath assemblies during 5 min as a result of interbacterial protein complementation was assessed for each indicated strain within 200 recipient cells displaying T6SS activity. Data are represented as mean ± SD.

(C) Time until the first detection of sheath assembly by interbacterial protein complementation was measured for each indicated strain co-incubated with T6SS$^+$ donor cells. Dashed line indicates time prior to imaging. Data are represented as mean ± SD.

(D and E) VgrG2 (D) or Hcp (E) was expressed from pBAD vectors in *vipA-msfGFP* background strains lacking *vgrG2* or *hcp1/hcp2*, respectively. The time after cells were spotted on a pad with 0.1% L-arabinose is indicated. Images show representative cells in GFP fluorescence channel to visualize sheath assembly. See Movie S5 for full time-lapse movies.

All data shown in this figure were acquired from three independent biological replicates. For statistical analysis one-way ANOVA with multiple comparison using Tuckey post hoc test was performed, *$p < 0.0001$; n.s., non-significant. Scale bar, 2 μm on all images.

See also Figure S5.

sufficient for sheath assembly; however, to fully restore T6SS activity, both Hcp and VgrG2 proteins have to be expressed to a level that is close to the wild-type level (Figure S5). Taken together, these observations suggest that during interbacterial protein complementation the frequency of assembly and sheath length are limited by the amount of Hcp and VgrG2 proteins delivered into the recipient cells.

T6SS Effectors Are Exchanged between Cells

Hcp secretion in *V. cholerae* was previously shown to be abolished in the absence of VgrG3 and VasX (Dong et al., 2013). We reasoned that this was likely a consequence of an aberrant T6SS assembly and created strains lacking *vgrG1*, *vgrG3*, and/or *vasX* in *vipA-msfGFP* background. Indeed, the frequency of sheath assembly was significantly decreased in strains lacking one or any combination of two of these three effectors. For example, deletion of *vgrG3* and *vasX* lowered T6SS activity 300-fold to a frequency of one sheath assembly in 100 cells and additional deletion of *vgrG1* further decreased the activity 10-fold (Figures 3A and S1). To test if the tip-associated effectors VgrG1, VgrG3, and VasX are also transferred between cells, we mixed *vgrG1/vgrG3/vasX* triple mutant recipient cells with T6SS$^+$ donor cells. Similarly to VgrG2 transfer, single sheath structures were first detected after 2 min and the average sheath length was indistinguishable from the sheath length in wild-type cells (Figures 2A–2C). Sheath assembly was restored also in *vgrG1/vgrG2/vgrG3* cells mixed with T6SS$^+$ donor cells (Figure 3B).

Sheath assembly in *vgrG1/vgrG3/vasX* triple mutant could be triggered either by transfer of a whole tip complex or any combination of VgrG1, VgrG3, or VasX effectors because the corresponding double or single mutants all assemble the sheath with a higher frequency than the triple mutant (Figure 3A). To test if transfer of VgrG3 effector alone could restore the activity, we mixed the triple effector mutant recipient cells with double mutant *vgrG1/vasX* donor cells, which transfer VgrG2/VgrG3 complex at approximately ten times lower rate than wild-type (Figure 3A; Movie S6). Indeed, the frequency of sheath assembly was significantly increased in the *vgrG1/vgrG3/vasX* recipient cells (Figures 3C and 3D; Movie S6). This suggests that in addition to VgrG2, the whole tip complex with associated effectors is transferred between cells and can be reused to initiate new T6SS assembly.

Translocated and Cytosolic Proteins Mix to Assemble Functional T6SS

To test if the T6SS assembled from complemented components is functional, we generated two reporter strains that are sensitive to delivery of T6SS substrates TseL (targets lipids) or VgrG3 (targets peptidoglycan) (Brooks et al., 2013; Dong et al., 2013; Unterweger

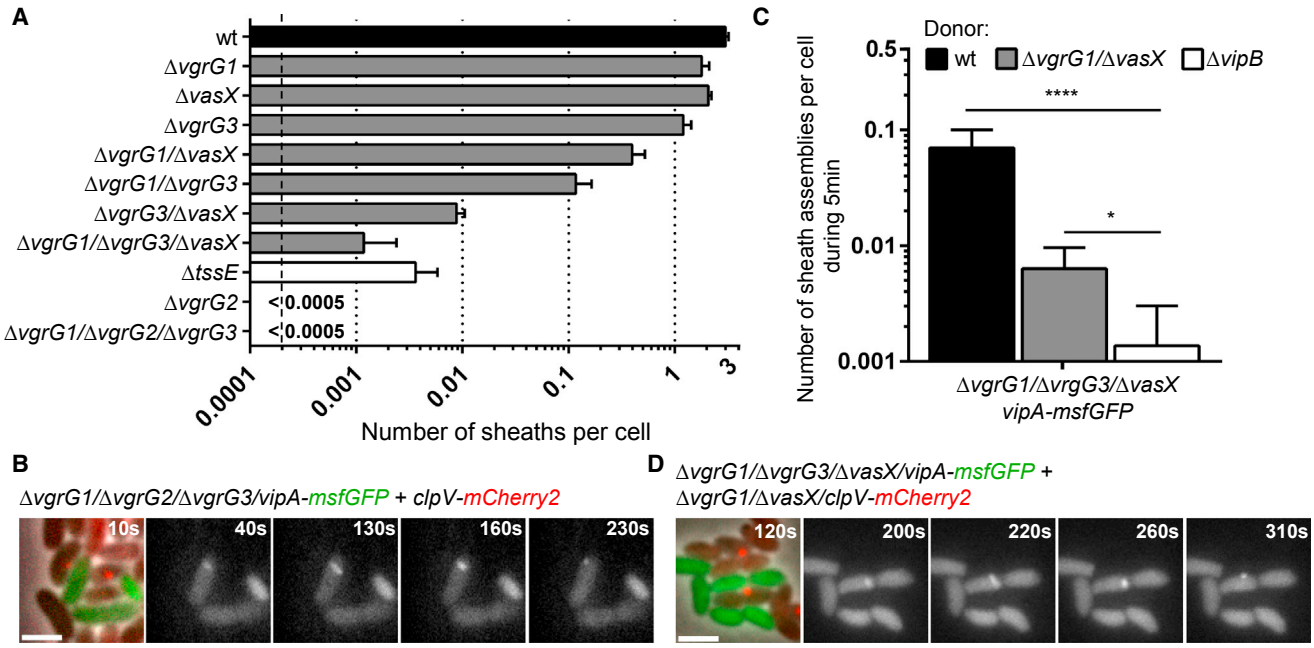

Figure 3. T6SS Effectors Are Efficiently Exchanged among Neighboring Cells

(A) Total number of sheath assemblies detected in 5,000 cells of each indicated strain (all *vipA-msfGFP* background) at a given point of time was divided by number of cells. Dashed line represents detection limit for this analysis and is given by number of analyzed cells. Black bar represents wild-type, gray bars represent strains lacking one or several T6SS effectors, white bars represent strains lacking a structural component. No structures were detected in 20,000 *vgrG2* and *vgrG1/vgrG2/vgrG3* triple mutants. Representative images can be found in Figure S1.

(B) Full VgrG tip interbacterial protein complementation: depicted are individual frames of a 5-min time-lapse. The first frame shows all cells and is a merge of phase contrast, GFP (*ΔvgrG1/ΔvgrG2/ΔvgrG3*, T6SS$^-$ recipient) and mCherry2 (wild-type donor) fluorescence channels. The following four frames only show GFP fluorescence channel to visualize sheath dynamics.

(C) Sheath assembly was monitored in the Δ*vgrG1/*Δ*vgrG3/*Δ*vasX/vipA-msfGFP* strain for 5 min after 30 min co-incubation either with *clpV-mCherry2* (wild-type T6SS activity), Δ*vgrG1/*Δ*vasX/clpV-mCherry2* (around 10× reduced T6SS activity), or Δ*vipB* (T6SS$^-$) donor cells. Total number of sheath assemblies was counted in at least 10,000 GFP$^+$ cells for indicated strains. **** $p < 0.0001$, * $p < 0.05$; one-way ANOVA and Tuckey post hoc test for multiple comparison.

(D) VgrG3-specific interbacterial protein complementation using *vgrG1/*Δ*vgrG3/*Δ*vasX* as recipient and Δ*vgrG1/*Δ*vasX* as donor. See Movie S6 for full time-lapse movie.

All data shown in this figure were acquired from three independent biological replicates and are represented as mean ± SD. Scale bar, 2 μm on all images.

et al., 2014). These reporter strains were used as donor cells in two different assays. In the first assay, we tested delivery of TseL from recipient cells into *tseL-tsiV1*-negative donor cells by monitoring their lysis (Figure 4A). The donor cells expressed LacZ from an inducible pBAD33 plasmid and the level of LacZ release was monitored by placing the donor-recipient cell mixture on an agar containing a cell impermeable substrate of LacZ, chlorophenol red-β-D-galactopyranoside (CPRG), which can be used to monitor integrity of LacZ$^+$ cells (Paradis-Bleau et al., 2014). Indeed, when such TseL-sensitive and LacZ$^+$ reporter cells were mixed with wild-type cells, the LacZ was released as documented by increase in 572 nm absorbance upon CPRG hydrolysis to chlorophenol red (Figures 4B and 4C). This was clearly a result of T6SS-dependent delivery of TseL because the CPRG conversion was abolished by deleting *vipB* or *tseL*. Interestingly, lysis of the T6SS$^+$ reporter cells was detected when the cells were mixed with *hcp1/hcp2*, *vgrG2*, or *vgrG2/hcp1/hcp2* recipient strains (Figures 4B and 4C). On the other hand, inactivating T6SS in the reporter cells blocked their lysis, confirming that the recipient cells lacking VgrG2 or Hcp are unable to lyse the reporter cells unless VgrG2 or Hcp proteins are first delivered from the reporter cells (Figure S2D).

To estimate the detection limit of the CPRG-based assay, we tested lysis of LacZ$^+$ *E. coli* and the *V. cholerae* reporter by *V. cholerae* lacking *tssE*. This mutant was previously shown to assemble the sheath with a low frequency but had undetectable killing activity using competition assays that measure survival of prey *E. coli* (Basler et al., 2012). Here, we show that in the absence of *tssE*, the sheath assembly rate decreased ~1,000-fold and on average only one sheath assembled per 300 cells (Figure 3A). When *tssE*-negative strain was mixed with *E. coli*, significant LacZ release was observed after 160 min of incubation on CPRG containing agar (Figure S2B). Similarly, significant lysis of *V. cholerae* reporter strain was observed after 160 min (Figure 4C). This confirms that the residual sheath assembly in *tssE*-negative strain is functional and the CPRG assay detects up to 1,000-fold decreased T6SS activity. Importantly, the cells lacking VgrG2 or Hcp were indistinguishable from a strain lacking VipB and induced no detectable lysis of *E. coli* even upon extended incubation (Figure S2B).

In the second assay, we tested VgrG3 translocation using a reporter strain lacking *vgrG3-tsiV3* (Figure 4D). When VgrG3-sensitive reporter cells were incubated with wild-type cells for 1 hr,

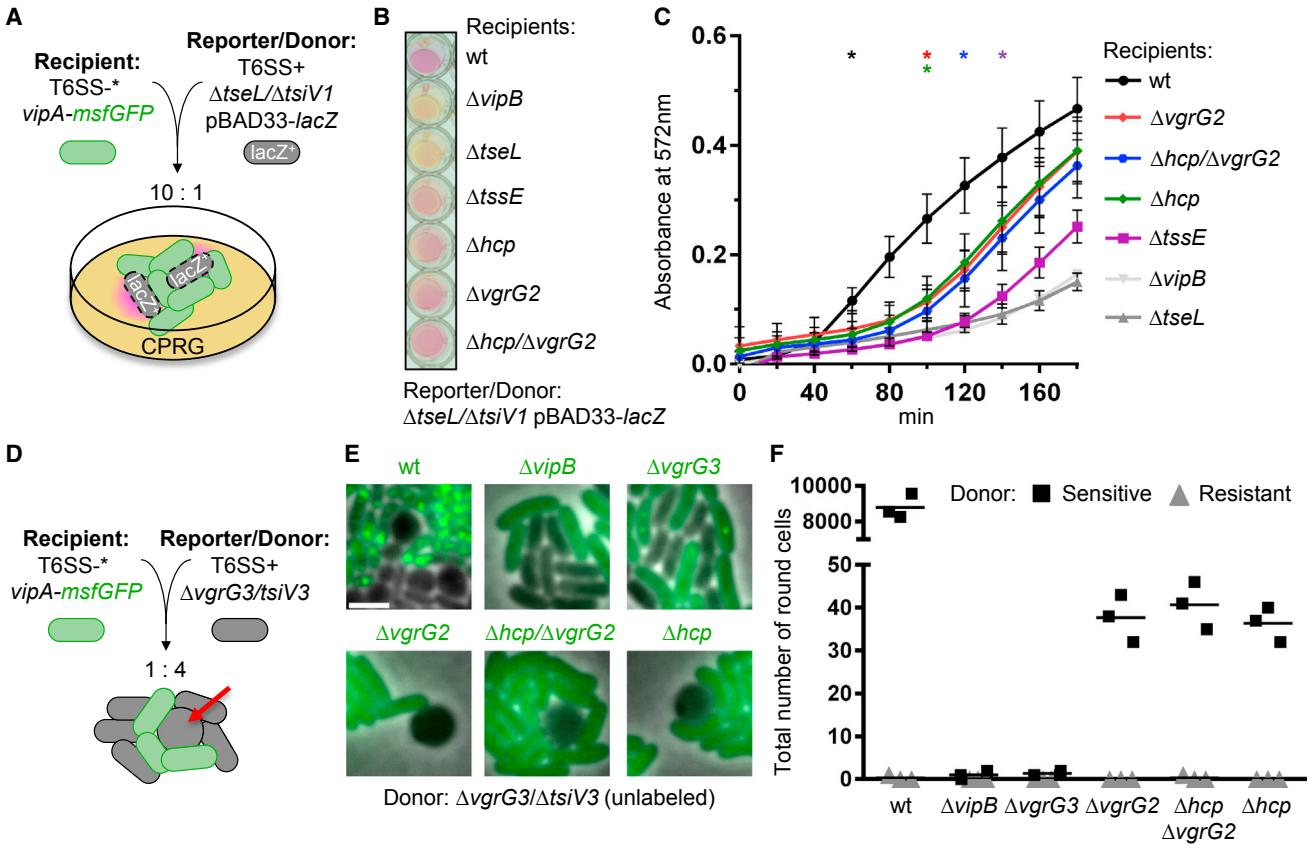

Figure 4. Translocated Proteins Are Reused to Form a Functional T6SS

(A) T6SS$^+$ donor cells lacking the effector TseL and its associated immunity protein TsiV1, as well as harboring the pBAD33-*lacZ* vector were used for interbacterial protein complementation assay. Cell mixtures were plated on a LB agar plate containing 20 μg/ml CPRG and 0.1% L-arabinose. Cell-impermeable CPRG is converted by released β-galactosidase to chlorophenol red with an absorbance maximum at 572 nm.

(B) A representative image of a CPRG-based cell permeability assay on 96-well plate is shown after 180 min co-incubation of indicated strains with LacZ$^+$ Δ*tseL/ΔtsiV1* donor strain.

(C) Indicated recipient strains were mixed with the donor strain and incubated for 3 hr at 37°C in 96-well plate. Absorbance was measured in 20 min intervals at 572 nm. Colored asterisks mark time point from which chlorophenol red absorbance was significantly higher as compared to background absorbance (Δ*vipB* + reporter) determined by unpaired t test.

(D) T6SS$^+$ donor cells lacking the effector VgrG3 and its associated immunity protein TsiV3 were used for interbacterial protein complementation. Bacterial mixtures were co-incubated on LB agarose pad under a glass coverslip for 1 hr prior to screening for cell-rounding.

(E) Representative images of cells are shown and are a merge of phase contrast and GFP fluorescence channels depicting cell-rounding in VgrG3-sensitive donor cells (black label, no fluorescence) and indicated *vipA-msfGFP* background strains (green label, GFP fluorescence). Scale bar, 2 μm.

(F) Cell-rounding was assessed in 40,000 donor cells being either sensitive (Δ*vgrG3/ΔtsiV3*, black squares) or resistant (Δ*vgrG3,* gray triangles) to VgrG3-specific T6SS attack from indicated recipient strain.

All data were acquired from three independent experiments and are represented as mean ± SD.

See also Figure S2.

approximately one in five reporter cells lost their characteristic curved-rod shape and rounded up (Figure 4E). No round cells were detected when wild-type cells were in close contact with wild-type sister cells or when the reporter cells were mixed with *vgrG3*- or *vipB*-deficient strains (Figures 4E and 4F). Interestingly, after 1 hr of incubation of *vgrG3/tsiV3*-negative cells, with *hcp1/hcp2* and/or *vgrG2*-negative recipient cells, ~1 in 1,000 sensitive cells were round (Figure 4F). The frequency of round cell formation dependent on protein complementation was ~200-fold lower than the frequency observed when wild-type cells were mixed with VgrG3-sensitive cells. This is, however, expected considering two important facts. First, as shown above, recipient cells assemble T6SS using *trans*-complemented proteins at a rate that is ~50-fold lower than that of wild-type cells (Figure 1H). Second, *vgrG3-tsiV3* donor strain has three times reduced T6SS dynamics compared to the wild-type donor cells and it is therefore also likely complementing VgrG2 and Hcp at three times lower rate (Figure 3A). When T6SS was inactivated in the donor cells, no cell rounding was observed (Figure S2E). As in the case of TseL, this excludes an alternative delivery mechanism of VgrG3 in the absence of VgrG2 or Hcp proteins in the recipient cells.

Taken together, these two assays clearly indicate that the T6SS assembly in the recipient cells resulting from interbacterial protein complementation of Hcp or VgrG2 is functional and can

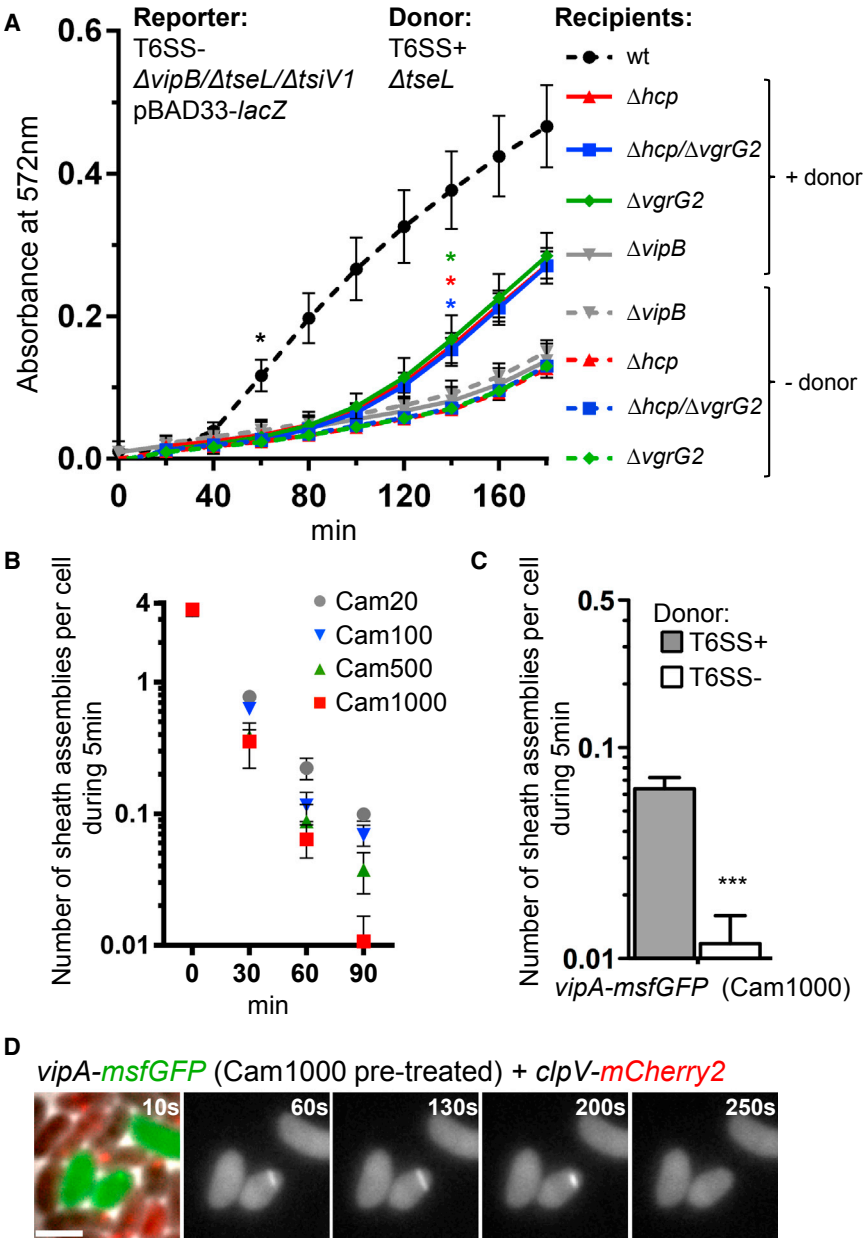

Figure 5. Cooperation Dependent on Interbacterial Protein Complementation

(A) T6SS$^+$ donor cells lacking the effector TseL and indicated recipient strains were mixed with a lipase-sensitive, T6SS$^-$, LacZ$^+$ reporter strain at a ratio of 5:5:1 (donor/recipient/reporter) for the detection of cell lysis. Dashed lines indicate co-incubation of only recipient and reporter strains in the absence of donor. Solid lines indicate a complete three strain mixture. Colored asterisks mark time point from which chlorophenol red absorbance was significantly higher as compared to background absorbance (Δ*vipB* + donor + reporter) determined by unpaired t test.

(B) Wild-type *vipA-msfGFP*-labeled *V. cholerae* cells were grown to an optical density (OD) of 0.8 prior to the addition of 20, 100, 500, or 1,000 μg/ml chloramphenicol to the culture and continued incubating (200 rpm, 37°C) for up to 90 min. At indicated time points a sample was taken for the analysis of T6SS activity. For each time point and antibiotic concentration, the sheath assemblies were counted in 500 cells.

(C) Sheath assembly was monitored in chloramphenicol-treated wild-type cells upon co-incubation with untreated T6SS$^+$ or T6SS$^-$ donor cells. Total number of sheath assemblies was counted for 5,000 GFP$^+$ cells.

(D) Interbacterial protein complementation in translationally inhibited cells. Depicted are individual frames of a 5-min time-lapse. The first frame shows all cells and is a merge of phase contrast, GFP (T6SS substrate-depleted wild-type, T6SS$^-$ recipient) and mCherry2 (untreated wild-type donor) fluorescence channels. The following four frames only show GFP fluorescence channel to visualize sheath dynamics. See Movie S7 for full time-lapse movie. Scale bar, 2 μm.

All data were acquired from three independent experiments and are represented as mean ± SD.

deliver both TseL and VgrG3 into neighboring target cells. Interestingly, these experiments also showed that the composition of the tip complex had to change after translocation. The donor cells lacked TseL or VgrG3, however, both TseL and VgrG3 were clearly secreted by the recipient cells after Hcp and VgrG2 complementation. This suggests that the tube-tip complex delivered by the donor cells disassembles after translocation into recipient cells and forms again during new T6SS assembly. Interestingly, Hcp complementation supports formation of T6SS capable of substrate delivery even though most sheath structures are shorter than wild-type (Figure 2A), suggesting that the full-length T6SS sheath is not strictly required for substrate delivery (Figures 4C and 4F).

Interbacterial Protein Complementation Increases Chances to Kill Competition

Exchange of secreted T6SS components between neighboring cells could provide a benefit to a bacterial community of strains with structurally compatible T6SSs. To test efficiency of such cooperation, we generated a reporter strain, which is only sensitive to TseL delivery and releases LacZ upon lysis, however, is itself unable to secrete any T6SS substrates. When such reporter strain was mixed with a strain that lacks TseL but is capable of delivering other T6SS substrates (donor), no reporter lysis was observed (Figure 5A). Similarly, if the reporter was mixed with a strain that expresses TseL but lacks the structural components Hcp or VgrG2 (recipient), no lysis was observed (Figure 5A). However, when all three strains (reporter, donor, and recipient) were mixed together LacZ was released from lysed reporter cells (Figure 5A). This indicates that donor cells translocated Hcp or VgrG2

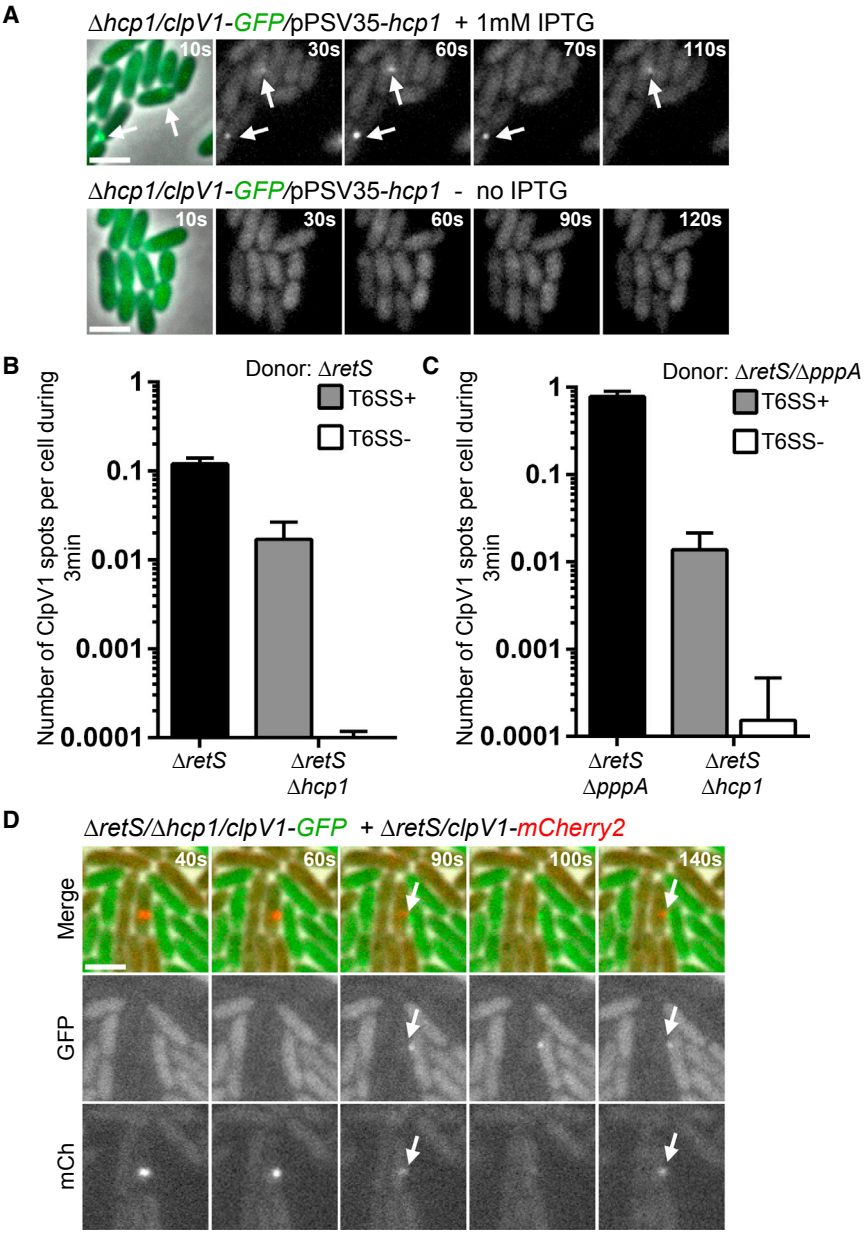

Figure 6. T6SS Mediated Hcp1 Complementation among *P. aeruginosa* Cells

(A) ClpV1-GFP-labeled cells lacking *hcp1* were complemented from pPSV35-*hcp1*. Protein expression was either induced by the addition of 1 mM IPTG for 1 hr at OD of 0.5 to the culture (top) or left uninduced (bottom). Subsequently cells were monitored for ClpV1 spot formation. Depicted are individual time points from a 3-min time-lapse movie. The first frame is a merge of phase contrast and GFP signal. The following four frames only show GFP fluorescence channel to visualize ClpV1 spots.

(B and C) Number of ClpV1 spots in 5,000 GFP$^+$ cells was monitored in the Δ*hcp1* strain (Δ*retS*/*clpV1-GFP* background) for 3 min after 45 min co-incubation either with T6SS$^+$ or T6SS$^-$ donor cells. Black bar indicates number of ClpV1 spots per cell in Δ*retS*/*clpV1-mCherry2* (B) or Δ*retS*/Δ*pppA*/*clpV1-mCherry2* (C) donor strain. Data are represented as mean ± SD and were acquired from four independent biological replicates.

(D) *P. aeruginosa* interbacterial protein complementation: Depicted are individual frames of a 3-min time-lapse. The top row shows all cells and is a merge of phase contrast, GFP (Δ*retS*/Δ*hcp1*, T6SS$^-$ recipient) and mCherry2 (Δ*retS* donor) fluorescence channels. The middle and bottom rows only show GFP and mCherry2 fluorescence channel respectively, to clearly identify ClpV1 spots. Arrows highlight ClpV1 spots in donor and recipient as a result of interbacterial protein complementation. Image series were corrected to reduce effects of photo-bleaching. See Movie S8 for complete time-lapse movie. Scale bar, 2 μm.

See also Figure S6.

proteins into the recipient cells that then used these proteins to deliver TseL into the reporter strain to lyse it. This experiment provides a proof of concept that in polymicrobial communities cooperation between two strains based on T6SS dependent protein exchange could contribute to killing of a third strain.

Many anti-bacterial toxins cleave RNA or DNA of target cells. This blocks protein synthesis and presumably decreases the ability of the cells to defend themselves. Indeed, when wild-type *V. cholerae* cells were incubated with chloramphenicol at increasing concentration for extended period of time, the number of sheath assemblies and thus T6SS activity decreased to up to 300 times lower levels (Figure 5B). Interestingly, when such cells were mixed with sister cells with active T6SS, the activity in the inhibited cells was partially restored (Figures 5C and 5D; Movie S7). This suggests that on-going protein translation is mainly required for synthesis of T6SS substrates and if this is inhibited, the available substrates are secreted out of the cells and T6SS activity decreases. Protein complementation from neighboring sister cells can however prolong T6SS activity and thus potentially increase the chance to successfully fight competition.

The Efficiency of T6SS-Dependent Protein Delivery Depends on Precise Aiming of T6SS

Activity of *P. aeruginosa* H1-T6SS, manifested by dynamic formation of ClpV1-GFP spots, is increased by deletion of *retS* and depends on presence of Hcp1 (Basler and Mekalanos, 2012; Mougous et al., 2006) (Figure 6A). The H1-T6SS assembly is regulated by the TagQRST/PpkA/PppA signaling cascade through phosphorylation and dephosphorylation of Fha1 protein (Basler et al., 2013; Mougous et al., 2007). Importantly, cells with the intact signaling cascade show only low level of H1-T6SS activity, however, can quickly assemble and subcellularly localize

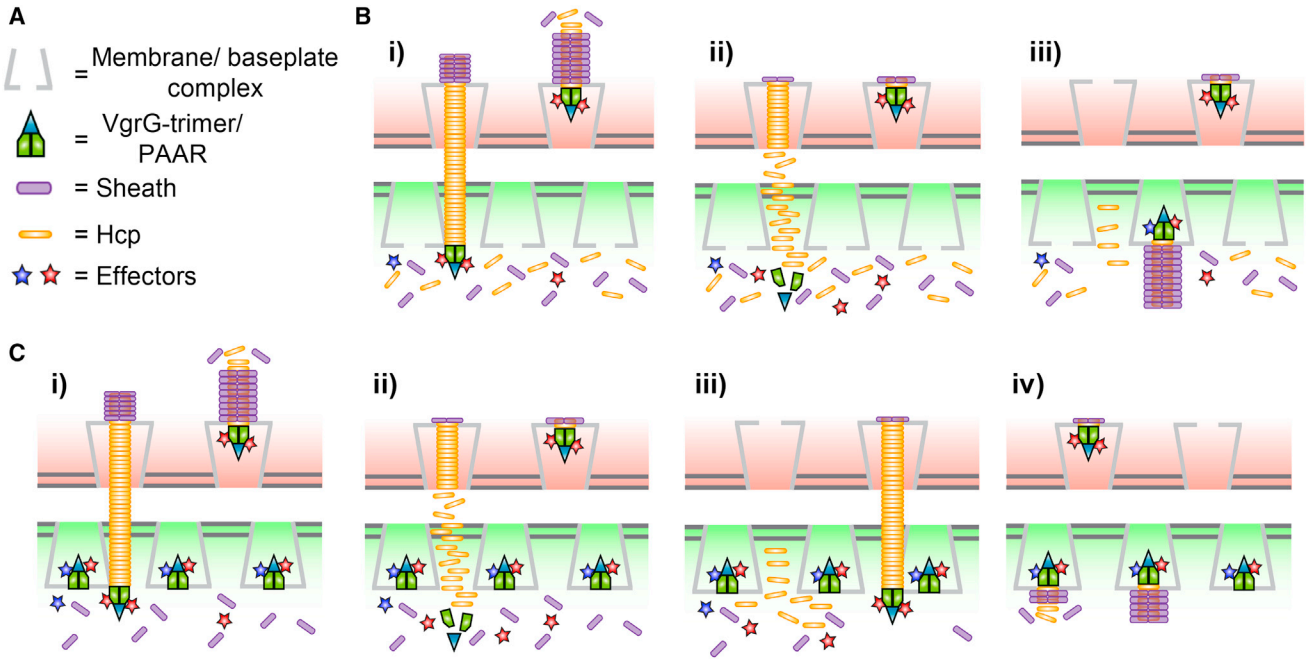

Figure 7. Model for Interbacterial Protein Complementation of Secreted T6SS Components

(A) Overview of depicted T6SS components (not shown in scale).

(B) Tip complementation. VgrGs and associated effectors are translocated from a T6SS^{+} donor cell (red shade) into a T6SS^{-} recipient cell (green shade) (i), the translocated tip structure rapidly dissociates (ii) and reassembles into a functional T6SS (iii). The assembly of a single full-length Hcp-sheath complex is initiated because sufficient Hcp and sheath subunits are available in the recipient cell and only single tip complex is formed. Translocated tip complexes dissociate in the recipient cells or can be modified by the addition of effector molecules prior to the next round of secretion.

(C) Hcp complementation. Multiple translocation events (i–iv) are needed during Hcp complementation to detect sheath assembly. Recycled Hcp subunits are used for several Hcp-sheath assemblies that are initiated from many functional baseplates, thus leading to multiple significantly shorter sheath assemblies. Hcp-tip complex dissociates in the recipient cells.

See also Figure S7.

their T6SS in the response to external stimuli. In the absence of phosphatase PppA, the T6SS assembly is constitutive, however, the cells are unable to efficiently reposition the H1-T6SS assembly and its subcellular localization seems constant (Basler et al., 2013; Ho et al., 2013). These properties of H1-T6SS allowed us to assess the role of T6SS aiming in T6SS-dependent protein transfer.

To estimate the efficiency Hcp1 transfer between *P. aeruginosa* cells, we mixed *retS/hcp1*-negative recipient strain (*clpV1-GFP* background) with *retS*-negative or *retS/pppA*-negative donor strains (*clpV1-mCherry2* background). After 45 min of co-incubation, ClpV1 localization was monitored for 3 min in both donor and recipient cells (Figures 6B–6D and S6). ClpV1-GFP spot formation was restored in 1.5% of the recipient cells mixed with either one of the two T6SS^{+} donors, but no ClpV1-GFP spots were detected in a control mixture with *retS/tssC1*- or *retS/pppA/tssB1*-negative donor cells (Figures 6B and 6C). This shows that *P. aeruginosa* is capable of exchanging Hcp1 in a T6SS-dependent manner. The efficiency of Hcp1 transfer was at least six times lower in the mixtures with *pppA*-negative donors than with *pppA*-positive donors because the T6SS activity in the recipients was the same despite the fact that the deletion of *pppA* increased the number of cells with ClpV1 spots more than six times from 12% to 78% (Figures 6B, 6C, and S6; Movie S8). This suggests that the ability to aim T6SS at the target cells is crucial for efficient effector delivery.

DISCUSSION

We show here that measuring frequency of sheath assembly by live-cell microscopy and lysis of target cells are sensitive methods to detect T6SS activity. We used these methods to provide evidence that secreted T6SS components, such as VgrG, Hcp, and effectors, are exchanged between neighboring cells in a T6SS-dependent manner and can be directly reused for a new assembly of a functional T6SS (Figure 7).

T6SS effector translocation was so far detected by live-cell imaging of morphological changes or lysis of target cells (Basler et al., 2013; Borenstein et al., 2015; Brunet et al., 2013; Ho et al., 2013; LeRoux et al., 2012). From these experiments it was, however, unclear how quickly and with what efficiency the T6SS substrates were translocated because the target cells had to be significantly damaged to detect any change. Similarly to phage, T6SS sheath polymerization is initiated by baseplate, which assembles around a single tip complex (Brunet et al., 2015; Durand et al., 2015; Leiman and Shneider, 2012; Taylor et al., 2016). Therefore, imaging sheath assembly in cells that lack tip proteins could detect a consequence of translocation

of a single tip complex from neighboring cells (Figure 7). Interestingly, we show that T6SS protein translocation can be detected already 2 min after mixing the donor and recipient *V. cholerae* cells (Figure 2C). Protein transfer efficiency can be up to 2% in cells with random localization of T6SS assembly but can be higher if T6SS is properly aimed at the target cells (Figures 1I, 3C, 5A, 6B, and 6C). This efficiency is higher than that of interbacterial protein transfer that was previously measured for T4SS substrates. Frequency of a recombination event upon transfer of a substrate protein fused to Cre recombinase was shown to be $\sim 10^{-3}$ for RP4-dependent MobA translocation and $<10^{-5}$ for Dot/Icm of *Legionella pneumophila* (Luo and Isberg, 2004).

The fact that Hcp and VgrG proteins can be reused for new T6SS assemblies together with the following observations suggest that the proteins are delivered into the cytosol of the target cells. Hcp protein was detected in all cellular fractions with the majority being in the cytosol (Lin et al., 2014; Mougous et al., 2007). T6SS tail assembly is similar to that of phage thus the tube subunits likely assemble on the end of the tube polymer that is distal to the baseplate (Brunet et al., 2014; Leiman and Shneider, 2012; Zoued et al., 2016). Because assembly of T6SS starts from membrane-associated baseplate complex and progresses across the whole cytosol (Durand et al., 2015), most, if not all, of the Hcp protein would be needed in the cytosol. The VgrG proteins were never detected in the periplasm and, similarly to Hcp, lack canonical secretion signal (Boyer et al., 2009). Furthermore, the recently resolved structure of the membrane complex shows that the periplasmic part the T6SS machine is rather small and tightly packed, which suggests that the secreted substrates are loaded onto the tip from the cytosol (Durand et al., 2015). Together, this indicates that VgrG, Hcp, and effectors are likely assembled onto the functional T6SS machine from the cytosol and therefore, at least during interbacterial protein complementation, both Hcp and VgrGs can be delivered to the cytosol of target cells (Figure 7). Our data support a parsimonious explanation that tip and Hcp proteins are directly translocated to the cytosol of target cells by T6SS. Even though another mechanism in the target cells may translocate Hcp and VgrGs from periplasm to the cytosol, such mechanism would have to be able to efficiently and quickly translocate both Hcp and VgrG proteins and be present in both *V. cholerae* and *P. aeruginosa*.

In a single layer of cells with random orientations of their T6SSs, most of the translocation events will likely miss target cells. Assuming that the reach of T6SS is up to a half width of a cell and taking the cell geometry into account, only a maximum of one in six events has a potential to hit a neighboring target cell (Figure S7) (Ho et al., 2014). The observed efficiency of protein complementation in *V. cholerae* is, however, lower, which suggests that only fraction of Hcp or tip secretion results in a new T6SS assembly in the cytosol. Indeed, T6SS may deliver substrates more frequently to the periplasm than to cytosol because many T6SS effectors, including both VgrG3 and TseL, target substrates in the periplasm (Brooks et al., 2013; Dong et al., 2013; Liang et al., 2015; Unterweger et al., 2014). Direct labeling of T6SS substrates or a method for detection of a single molecule transfer is needed for precise quantification of delivery to cytosol and periplasm, however, it is likely that the T6SS substrates are stochastically delivered to both periplasm and cytosol. The approaches developed in this study will allow further understanding of T6SS-dependent protein transfer.

STAR★METHODS

Detailed methods are provided in the online version of this paper and include the following:

- KEY RESOURCES TABLE
- CONTACT FOR REAGENT AND RESOURCE SHARING
- EXPERIMENTAL MODEL AND SUBJECT DETAILS
  - Bacterial Strains and Growth Conditions
- METHOD DETAILS
  - DNA Manipulations
  - Bacterial Competition Assays
  - Antibodies
  - Western Blotting
  - Fluorescence Microscopy
  - Chloramphenicol Depletion of T6SS-Positive Cells
  - Image Analysis
- QUANTIFICATION AND STATISTICAL ANALYSIS

SUPPLEMENTAL INFORMATION

Supplemental Information includes seven figures, one table, and eight movies and can be found with this article online at http://dx.doi.org/10.1016/j.cell.2016.08.023.

A video abstract is available at http://dx.doi.org/10.1016/j.cell.2016.08.023#mmc10.

AUTHOR CONTRIBUTIONS

A.V. designed and performed the experiments, analyzed and interpreted the data, and wrote the manuscript. M.B. designed the experiments, analyzed and interpreted the data, and wrote the manuscript.

ACKNOWLEDGMENTS

We thank Mihai Ionescu for an excellent technical assistance in obtaining Hcp antibody. The work was supported by SNSF Starting Grant BSSGI0_155778 and the University of Basel. A.V. was supported by the Biozentrum Basel International PhD Program "Fellowships for Excellence."

Received: March 3, 2016
Revised: June 29, 2016
Accepted: August 12, 2016
Published: September 8, 2016

REFERENCES

Alcoforado Diniz, J., Liu, Y.-C., and Coulthurst, S.J. (2015). Molecular weaponry: diverse effectors delivered by the Type VI secretion system. Cell. Microbiol. *17*, 1742–1751.

Basler, M., and Mekalanos, J.J. (2012). Type 6 secretion dynamics within and between bacterial cells. Science *337*, 815.

Basler, M., Pilhofer, M., Henderson, G.P., Jensen, G.J., and Mekalanos, J.J. (2012). Type VI secretion requires a dynamic contractile phage tail-like structure. Nature *483*, 182–186.

Basler, M., Ho, B.T., and Mekalanos, J.J. (2013). Tit-for-tat: type VI secretion system counterattack during bacterial cell-cell interactions. Cell *152*, 884–894.

Bina, X.R., Wong, E.A., Bina, T.F., and Bina, J.E. (2014). Construction of a tetracycline inducible expression vector and characterization of its use in *Vibrio cholerae*. Plasmid *76*, 87–94.

Bönemann, G., Pietrosiuk, A., Diemand, A., Zentgraf, H., and Mogk, A. (2009). Remodelling of VipA/VipB tubules by ClpV-mediated threading is crucial for type VI protein secretion. EMBO J. *28*, 315–325.

Borenstein, D.B., Ringel, P., Basler, M., and Wingreen, N.S. (2015). Established microbial colonies can survive Type VI secretion assault. PLoS Comput. Biol. *11*, e1004520.

Borgeaud, S., Metzger, L.C., Scrignari, T., and Blokesch, M. (2015). The type VI secretion system of *Vibrio cholerae* fosters horizontal gene transfer. Science *347*, 63–67.

Boyer, F., Fichant, G., Berthod, J., Vandenbrouck, Y., and Attree, I. (2009). Dissecting the bacterial type VI secretion system by a genome wide in silico analysis: what can be learned from available microbial genomic resources? BMC Genomics *10*, 104.

Brooks, T.M., Unterweger, D., Bachmann, V., Kostiuk, B., and Pukatzki, S. (2013). Lytic activity of the *Vibrio cholerae* type VI secretion toxin VgrG-3 is inhibited by the antitoxin TsaB. J. Biol. Chem. *288*, 7618–7625.

Brunet, Y.R., Espinosa, L., Harchouni, S., Mignot, T., and Cascales, E. (2013). Imaging type VI secretion-mediated bacterial killing. Cell Rep. *3*, 36–41.

Brunet, Y.R., Hénin, J., Celia, H., and Cascales, E. (2014). Type VI secretion and bacteriophage tail tubes share a common assembly pathway. EMBO Rep. *15*, 315–321.

Brunet, Y.R., Zoued, A., Boyer, F., Douzi, B., and Cascales, E. (2015). The Type VI secretion TssEFGK-VgrG phage-like baseplate is recruited to the TssJLM membrane complex via multiple contacts and serves as assembly platform for tail tube/sheath polymerization. PLoS Genet. *11*, e1005545.

Cianfanelli, F.R., Monlezun, L., and Coulthurst, S.J. (2016). Aim, load, fire: the Type VI secretion system, a bacterial nanoweapon. Trends Microbiol. *24*, 51–62.

Clemens, D.L., Ge, P., Lee, B.-Y., Horwitz, M.A., and Zhou, Z.H. (2015). Atomic structure of T6SS reveals interlaced array essential to function. Cell *160*, 940–951.

Dong, T.G., Ho, B.T., Yoder-Himes, D.R., and Mekalanos, J.J. (2013). Identification of T6SS-dependent effector and immunity proteins by Tn-seq in *Vibrio cholerae*. Proc. Natl. Acad. Sci. USA *110*, 2623–2628.

Durand, E., Cambillau, C., Cascales, E., and Journet, L. (2014). VgrG, Tae, Tle, and beyond: the versatile arsenal of Type VI secretion effectors. Trends Microbiol. *22*, 498–507.

Durand, E., Nguyen, V.S., Zoued, A., Logger, L., Péhau-Arnaudet, G., Aschtgen, M.-S., Spinelli, S., Desmyter, A., Bardiaux, B., Dujeancourt, A., et al. (2015). Biogenesis and structure of a type VI secretion membrane core complex. Nature *523*, 555–560.

Flaugnatti, N., Le, T.T.H., Canaan, S., Aschtgen, M.-S., Nguyen, V.S., Blangy, S., Kellenberger, C., Roussel, A., Cambillau, C., Cascales, E., and Journet, L. (2016). A phospholipase A1 antibacterial Type VI secretion effector interacts directly with the C-terminal domain of the VgrG spike protein for delivery. Mol. Microbiol. *99*, 1099–1118.

French, C.T., Toesca, I.J., Wu, T.-H., Teslaa, T., Beaty, S.M., Wong, W., Liu, M., Schröder, I., Chiou, P.-Y., Teitell, M.A., and Miller, J.F. (2011). Dissection of the *Burkholderia* intracellular life cycle using a photothermal nanoblade. Proc. Natl. Acad. Sci. USA *108*, 12095–12100.

Gerc, A.J., Diepold, A., Trunk, K., Porter, M., Rickman, C., Armitage, J.P., Stanley-Wall, N.R., and Coulthurst, S.J. (2015). Visualization of the *Serratia* Type VI secretion system reveals unprovoked attacks and dynamic assembly. Cell Rep. *12*, 2131–2142.

Guzman, L.M., Belin, D., Carson, M.J., and Beckwith, J. (1995). Tight regulation, modulation, and high-level expression by vectors containing the arabinose PBAD promoter. J. Bacteriol. *177*, 4121–4130.

Hachani, A., Allsopp, L.P., Oduko, Y., and Filloux, A. (2014). The VgrG proteins are "à la carte" delivery systems for bacterial type VI effectors. J. Biol. Chem. *289*, 17872–17884.

Hachani, A., Wood, T.E., and Filloux, A. (2016). Type VI secretion and anti-host effectors. Curr. Opin. Microbiol. *29*, 81–93.

Ho, B.T., Basler, M., and Mekalanos, J.J. (2013). Type 6 secretion system-mediated immunity to type 4 secretion system-mediated gene transfer. Science *342*, 250–253.

Ho, B.T., Dong, T.G., and Mekalanos, J.J. (2014). A view to a kill: the bacterial type VI secretion system. Cell Host Microbe *15*, 9–21.

Hood, R.D., Singh, P., Hsu, F., Güvener, T., Carl, M.A., Trinidad, R.R.S., Silverman, J.M., Ohlson, B.B., Hicks, K.G., Plemel, R.L., et al. (2010). A type VI secretion system of *Pseudomonas aeruginosa* targets a toxin to bacteria. Cell Host Microbe *7*, 25–37.

Kapitein, N., Bönemann, G., Pietrosiuk, A., Seyffer, F., Hausser, I., Locker, J.K., and Mogk, A. (2013). ClpV recycles VipA/VipB tubules and prevents non-productive tubule formation to ensure efficient type VI protein secretion. Mol. Microbiol. *87*, 1013–1028.

Koskiniemi, S., Lamoureux, J.G., Nikolakakis, K.C., t'Kint de Roodenbeke, C., Kaplan, M.D., Low, D.A., and Hayes, C.S. (2013). Rhs proteins from diverse bacteria mediate intercellular competition. Proc. Natl. Acad. Sci. USA *110*, 7032–7037.

Kudryashev, M., Wang, R.Y.-R., Brackmann, M., Scherer, S., Maier, T., Baker, D., DiMaio, F., Stahlberg, H., Egelman, E.H., and Basler, M. (2015). Structure of the type VI secretion system contractile sheath. Cell *160*, 952–962.

Leiman, P.G., and Shneider, M.M. (2012). Contractile tail machines of bacteriophages. Adv. Exp. Med. Biol. *726*, 93–114.

LeRoux, M., De Leon, J.A., Kuwada, N.J., Russell, A.B., Pinto-Santini, D., Hood, R.D., Agnello, D.M., Robertson, S.M., Wiggins, P.A., and Mougous, J.D. (2012). Quantitative single-cell characterization of bacterial interactions reveals type VI secretion is a double-edged sword. Proc. Natl. Acad. Sci. USA *109*, 19804–19809.

Liang, X., Moore, R., Wilton, M., Wong, M.J.Q., Lam, L., and Dong, T.G. (2015). Identification of divergent type VI secretion effectors using a conserved chaperone domain. Proc. Natl. Acad. Sci. USA *112*, 9106–9111.

Lin, J.-S., Wu, H.-H., Hsu, P.-H., Ma, L.-S., Pang, Y.-Y., Tsai, M.-D., and Lai, E.-M. (2014). Fha interaction with phosphothreonine of TssL activates type VI secretion in *Agrobacterium tumefaciens*. PLoS Pathog. *10*, e1003991.

Luo, Z.-Q., and Isberg, R.R. (2004). Multiple substrates of the *Legionella pneumophila* Dot/Icm system identified by interbacterial protein transfer. Proc. Natl. Acad. Sci. USA *101*, 841–846.

Ma, L.-S., Hachani, A., Lin, J.-S., Filloux, A., and Lai, E.-M. (2014). *Agrobacterium tumefaciens* deploys a superfamily of type VI secretion DNase effectors as weapons for interbacterial competition in planta. Cell Host Microbe *16*, 94–104.

MacIntyre, D.L., Miyata, S.T., Kitaoka, M., and Pukatzki, S. (2010). The *Vibrio cholerae* type VI secretion system displays antimicrobial properties. Proc. Natl. Acad. Sci. USA *107*, 19520–19524.

Metcalf, W.W., Jiang, W., Daniels, L.L., Kim, S.K., Haldimann, A., and Wanner, B.L. (1996). Conditionally replicative and conjugative plasmids carrying *lacZ* alpha for cloning, mutagenesis, and allele replacement in bacteria. Plasmid *35*, 1–13.

Miyata, S.T., Bachmann, V., and Pukatzki, S. (2013). Type VI secretion system regulation as a consequence of evolutionary pressure. J. Med. Microbiol. *62*, 663–676.

Mougous, J.D., Cuff, M.E., Raunser, S., Shen, A., Zhou, M., Gifford, C.A., Goodman, A.L., Joachimiak, G., Ordoñez, C.L., Lory, S., et al. (2006). A virulence locus of *Pseudomonas aeruginosa* encodes a protein secretion apparatus. Science *312*, 1526–1530.

Mougous, J.D., Gifford, C.A., Ramsdell, T.L., and Mekalanos, J.J. (2007). Threonine phosphorylation post-translationally regulates protein secretion in *Pseudomonas aeruginosa*. Nat. Cell Biol. *9*, 797–803.

Paradis-Bleau, C., Kritikos, G., Orlova, K., Typas, A., and Bernhardt, T.G. (2014). A genome-wide screen for bacterial envelope biogenesis mutants identifies a novel factor involved in cell wall precursor metabolism. PLoS Genet. *10*, e1004056.

Pietrosiuk, A., Lenherr, E.D., Falk, S., Bönemann, G., Kopp, J., Zentgraf, H., Sinning, I., and Mogk, A. (2011). Molecular basis for the unique role of the AAA+ chaperone ClpV in type VI protein secretion. J. Biol. Chem. *286*, 30010–30021.

Pukatzki, S., Ma, A.T., Sturtevant, D., Krastins, B., Sarracino, D., Nelson, W.C., Heidelberg, J.F., and Mekalanos, J.J. (2006). Identification of a conserved bacterial protein secretion system in *Vibrio cholerae* using the *Dictyostelium* host model system. Proc. Natl. Acad. Sci. USA *103*, 1528–1533.

Pukatzki, S., Ma, A.T., Revel, A.T., Sturtevant, D., and Mekalanos, J.J. (2007). Type VI secretion system translocates a phage tail spike-like protein into target cells where it cross-links actin. Proc. Natl. Acad. Sci. USA *104*, 15508–15513.

Rietsch, A., Vallet-Gely, I., Dove, S.L., and Mekalanos, J.J. (2005). ExsE, a secreted regulator of type III secretion genes in *Pseudomonas aeruginosa*. Proc. Natl. Acad. Sci. USA *102*, 8006–8011.

Russell, A.B., Peterson, S.B., and Mougous, J.D. (2014). Type VI secretion system effectors: poisons with a purpose. Nat. Rev. Microbiol. *12*, 137–148.

Schindelin, J., Arganda-Carreras, I., Frise, E., Kaynig, V., Longair, M., Pietzsch, T., Preibisch, S., Rueden, C., Saalfeld, S., Schmid, B., et al. (2012). Fiji: an open-source platform for biological-image analysis. Nat. Methods *9*, 676–682.

Shneider, M.M., Buth, S.A., Ho, B.T., Basler, M., Mekalanos, J.J., and Leiman, P.G. (2013). PAAR-repeat proteins sharpen and diversify the type VI secretion system spike. Nature *500*, 350–353.

Silverman, J.M., Brunet, Y.R., Cascales, E., and Mougous, J.D. (2012). Structure and regulation of the type VI secretion system. Annu. Rev. Microbiol. *66*, 453–472.

Taylor, N.M.I., Prokhorov, N.S., Guerrero-Ferreira, R.C., Shneider, M.M., Browning, C., Goldie, K.N., Stahlberg, H., and Leiman, P.G. (2016). Structure of the T4 baseplate and its function in triggering sheath contraction. Nature *533*, 346–352.

Unterweger, D., Miyata, S.T., Bachmann, V., Brooks, T.M., Mullins, T., Kostiuk, B., Provenzano, D., and Pukatzki, S. (2014). The *Vibrio cholerae* type VI secretion system employs diverse effector modules for intraspecific competition. Nat. Commun. *5*, 3549.

Whitney, J.C., Quentin, D., Sawai, S., LeRoux, M., Harding, B.N., Ledvina, H.E., Tran, B.Q., Robinson, H., Goo, Y.A., Goodlett, D.R., et al. (2015). An interbacterial NAD(P)(+) glycohydrolase toxin requires elongation factor Tu for delivery to target cells. Cell *163*, 607–619.

Zoued, A., Brunet, Y.R., Durand, E., Aschtgen, M.-S., Logger, L., Douzi, B., Journet, L., Cambillau, C., and Cascales, E. (2014). Architecture and assembly of the Type VI secretion system. Biochim. Biophys. Acta *1843*, 1664–1673.

Zoued, A., Durand, E., Brunet, Y.R., Spinelli, S., Douzi, B., Guzzo, M., Flaugnatti, N., Legrand, P., Journet, L., Fronzes, R., et al. (2016). Priming and polymerization of a bacterial contractile tail structure. Nature *531*, 59–63.

STAR★METHODS

KEY RESOURCES TABLE

REAGENT or RESOURCE	SOURCE	IDENTIFIER
Antibodies		
Rabbit polyclonal anti-Hcp	This paper	N/A
Rabbit polyclonal anti-VgrG2	This paper	N/A
Rabbit polyclonal anti-VipB	(Kudryashev et al., 2015)	N/A
Chemicals, Peptides, and Recombinant Proteins		
Streptomycin	AppliChem	A1852,0052; CAS: 3810-74-0
Ampicillin	AppliChem	A0839,0025; CAS: 69-52-3
Chloramphenicol	Sigma Aldrich	C1919; CAS: 56-75-7
Gentamicin	AppliChem	A1492,0025; CAS: 1405-41-0
Chlorophenol red-β-D-galactopyranoside	Sigma-Aldrich	59767-100MG-F; CAS: 99792-79-7
L-(+)-Arabinose	Sigma-Aldrich	A3256-25G; CAS: 5328-37-0
Isopropyl β-D-1-thiogalactopyranoside	AppliChem	A1008,0005; CAS: 367-93-1
Experimental Models: Organisms/Strains		
Vibrio cholerae 2740-80	(Basler et al., 2012)	PRJNA18253
Pseudomonas aeruginosa PAO1	(Mougous et al., 2006)	PRJNA331
A detailed strain list can be found in Table S1A.	this study	N/A
Recombinant DNA		
A detailed plasmid list can be found in Table S1B.	this study	N/A
Software and Algorithms		
Fiji	(Schindelin et al., 2012)	https://fiji.sc/
GraphPad Prism	http://www.graphpad.com	version 6.05 Windows
Other		
Nikon Ti-E inverted motorized microscope	Visitron	N/A

CONTACT FOR REAGENT AND RESOURCE SHARING

Further information and requests for reagents may be directed to, and will be fulfilled by the corresponding author Marek Basler (marek.basler@unibas.ch).

EXPERIMENTAL MODEL AND SUBJECT DETAILS

Bacterial Strains and Growth Conditions

A detailed strain list used in this study can be found in Table S1A. Bacteria were grown in Luria-Bertani (LB) broth at 37°C. Liquid cultures were grown aerobically. Antibiotic concentrations used were streptomycin (100 μg/ml), ampicillin (200 μg/ml), chloramphenicol (20 μg/ml) and gentamicin (15 μg/ml).

METHOD DETAILS

DNA Manipulations

All in-frame deletions and chromosomal mutations were generated by allelic exchange method using suicide plasmids pWM91 (*V. cholerae*) or pEXG2 (*P. aeruginosa*) (Metcalf et al., 1996; Rietsch et al., 2005). A list of plasmids and sequences of the peptides that replaced the indicated genes can be found in Table S1B. For plasmid complementation experiments in *V. cholerae* standard techniques were used to clone *hcp2* and *vgrG2* into L-arabinose inducible vectors pBAD24 and pBAD33 respectively (Guzman et al., 1995). For the detection of T6SS-mediated lysis in *V. cholerae*, *lacZ* was re-cloned from pXB308 (Bina et al., 2014) into pBAD33. For plasmid complementation in *P. aeruginosa*, *hcp1* was cloned into IPTG inducible vector pPSV35 (Rietsch et al., 2005). All cloning products were sequence verified. Chromosomal mutations were verified by PCR using primers outside of the replaced region.

Bacterial Competition Assays

For quantitative killing assays, bacteria were diluted from overnight culture 1:1000 (*V. cholerae*) or 1:200 (*E. coli*) into fresh LB medium supplemented with the appropriate antibiotics and incubated shaking at 37°C, 200 rpm. If indicated, protein expression was induced at OD = 0.2 by the addition of 0.1% L-arabinose to the culture. Bacteria were harvested at OD ≈1 and concentrated 10 times, mixed at ratio of 10:1 (*V. cholerae* to *E. coli*) and incubated on dry LB plates for 2 hr at 37°C. Surviving bacteria were counted by 10-fold serial dilutions on selective recovery plates (streptomycin for *V. cholerae*, gentamicin for *E. coli*). Three independent biological replicates were analyzed.

For the detection of T6SS mediated lysis of target cells a LacZ based detection assay was used. Lipase sensitive *V. cholerae* donor strain (*ΔtseL-ΔtsiV1*) harboring the pBAD33-*lacZ* vector was grown in the presence of 10 μg/ml chloramphenicol until OD ≈1, washed once and resuspended in 1 ml LB. Recipient cells were grown until OD ≈1 and concentrated 10 times. Indicated strains were mixed at a ratio of 10:1 (T6SS- recipients to *ΔtseL-ΔtsiV1*, LacZ+, T6SS+ donors), and 3 μl of the mixtures were spotted on dry 96-well LB plates containing 100 μl of LB agar supplemented with 20 μg/ml CPRG and 0.1% L-arabinose. For three strain lysis assays, strains were mixed at a ratio of 5:5:1 (recipient/donor/reporter). For the detection of *E. coli* lysis, strains were incubated on CPRG plates containing 100 μM IPTG for the induction of β-galactosidase. Bacteria were incubated up to 4 hr at 37°C and absorbance of chlorophenol red was measured every 20 min at 572 nm using an Epoch-2 plate reader (BioTek).

Antibodies

Antigen-purified rabbit polyclonal antibodies raised against VgrG2 peptide NGDPDQPIITGRTY and recombinant full-length Hcp protein were obtained commercially (GenScript, USA). Specificity of the antibodies was tested on *V. cholerae* strains expressing or lacking VgrG2 or Hcp, respectively.

Western Blotting

Bacteria were cultivated as described for the bacterial killing assay. For detection of secreted proteins 450 μl culture supernatant were concentrated by TCA/acetone precipitation, separated on Novex 4%–12% Bis-Tris SDS-PAGE gels (Life Technologies), and transferred to nitrocellulose membrane for immuno-detection. Primary antibodies were used at final concentration of 1 μg/ml in 5% milk in Tris buffered saline (pH 7.4) containing Tween 0.1% (TBST). Primary antibodies were incubated for 1.5 hr with horseradish peroxidase-labeled anti-rabbit antibody (Jackson Lab), washed with TBST, and peroxidase was detected by LumiGLO Chemiluminescent Substrate (Cell Signaling Technology, USA) on a gel imager (GE ImageQuant LAS 4000).

Fluorescence Microscopy

For interbacterial protein complementation experiments overnight cultures were washed once in LB and diluted 1:100 into fresh medium supplemented with appropriated antibiotics, and cultivated to an optical density (OD) at 600 nm of about 0.8–1.2. Cells from 1 ml of the culture were concentrated to OD 10, mixed at a ratio of 1:4 (recipient to donor), subsequently spotted on a thin pad of 1% agarose in LB and covered with a glass coverslip. Bacteria were immediately imaged during an observation period of 2 hr at 25°C using a Nikon Ti-E inverted motorized microscope with Perfect Focus System and Plan Apo 1003 Oil Ph3 DM (NA 1.4) objective lens. SPECTRA X light engine (Lumencore), ET-GFP (Chroma #49002) and ET-mCherry (Chroma #49008) filter sets were used to excite and filter fluorescence. sCMOS camera pco.edge 4.2 (PCO, Germany) (pixel size 65 nm) and VisiView software (Visitron Systems,Germany) were used to record images. Humidity was regulated to 95% using an Okolab T-unit (Okolab). For trans-complementation experiments from pBAD vectors, protein expression was induced by placing cells on a LB 1% agarose pad containing 0.1% L-arabinose. In *P. aeruginosa* protein induction from pPSV35 vector was induced by the addition of 1 mM IPTG to bacterial culture. Bacteria were immediately imaged during an observation period of 2 hr at 25°C. For functional testing of interbacterial protein complementation of secreted T6SS components, *V. cholerae ΔvgrG3/tsiV3* were used as donor cells and mixed with recipient strains as indicated. Prior to screening for cell-rounding, cells were incubated for 1 hr at 37°C.

Chloramphenicol Depletion of T6SS-Positive Cells

Wild-type *vipA-msfGFP* labeled bacteria were grown to an OD of 0.8 prior to the addition of up to 1 mg/ml chloramphenicol (diluted from stock of 200 mg/mL in 100% DMSO) to the culture. Cells were incubated further for 90 min and then 1 ml of culture was harvested and washed three times in 1 ml LB and subsequently concentrated to OD 10. Translationally inhibited cells were then mixed with untreated donor cells for interbacterial protein complementation assay. The final concertation of DMSO during 90 min chloramphenicol pre-incubation was up to 5%, which had no significant influence on T6SS sheath dynamics.

Image Analysis

Fiji (Schindelin et al., 2012) was used for all image analysis and manipulations. For quantification of T6SS activity total cell number was assessed from phase contrast image using the "find maxima" options with noise tolerance setting set to 3000. GFP positive cells were counted the same way using a noise tolerance setting of 250. Sheath number was assessed using a noise tolerance setting of 400. All quantifications were verified manually and carried out using the "edge maxima exclusion" function. For quantification of T6SS activity from time-lapse movies the "temporal color code" function was used. This procedure allows to reliably identifying low-frequency events such as sheath assembly by interbacterial protein complementation but becomes more imprecise with

increasing frequency (e.g., estimation of wild-type T6SS activity) due to overlapping signals. Sheath length measurements were performed exclusively on fully extended structures using the "straight line" tool in Fiji. Contrast on compared sets of images was adjusted equally. All imaging experiments were performed with at least three biological replicates.

QUANTIFICATION AND STATISTICAL ANALYSIS

Statistical parameters such as number of biological replicates and total analyzed bacteria as well as levels of significance are reported in the figure legends. Unpaired t test, ordinary one-way ANOVA or two-way ANOVA with multiple comparisons and Tuckey post hoc test was used to determine significance between all groups using GraphPad Prism version 6.05. If not indicated differently, data are represented as mean ± standard deviation (SD).

Cell

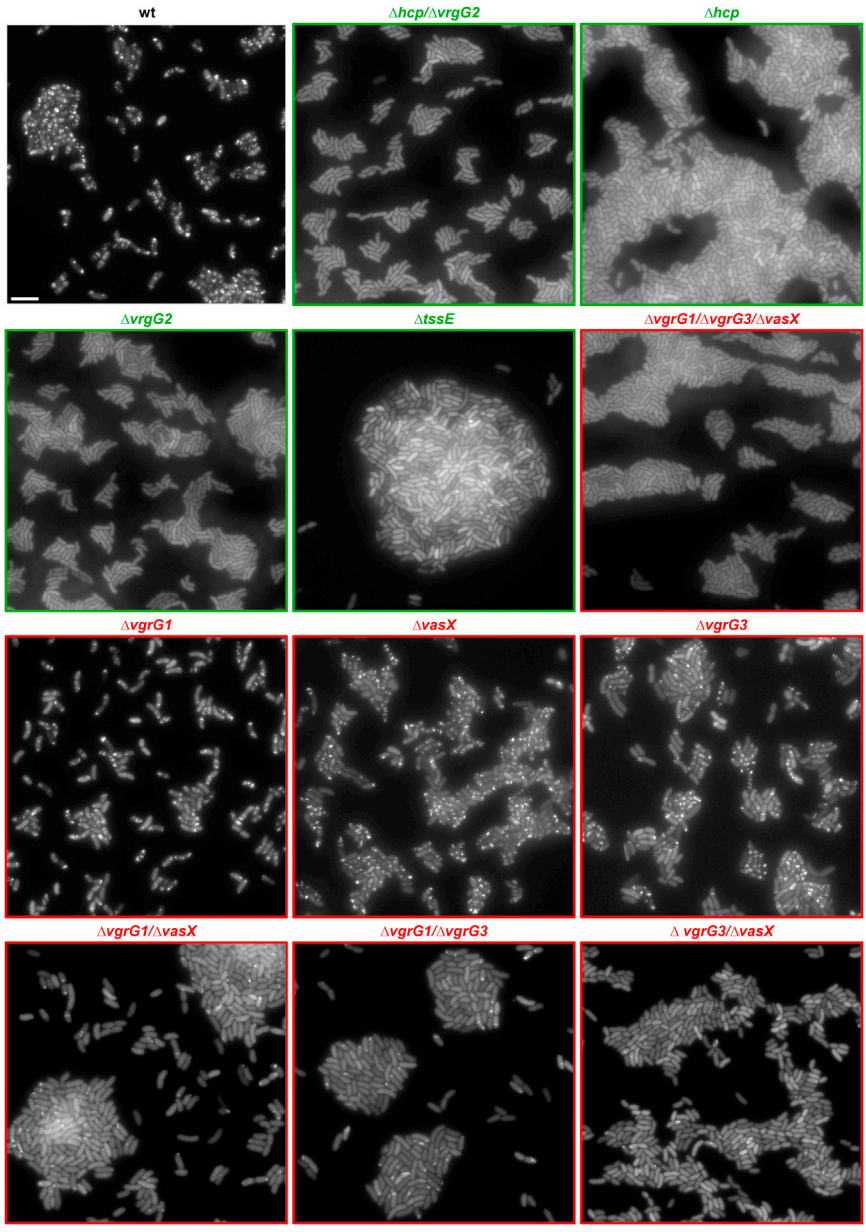

Figure S1. The Deletion of Secreted Structural Components and Effector Proteins Leads to a Complete Absence or Reduced Rate of Sheath Assembly, Related to Figures 1A and 3A

Depicted are representative 50 × 50 μm fields of GFP fluorescence channel for each indicated strain (all *vipA-msfGFP* background). Green label/frame indicates structural components. Red label/frame indicates effector proteins. Scale bar = 5 μm.

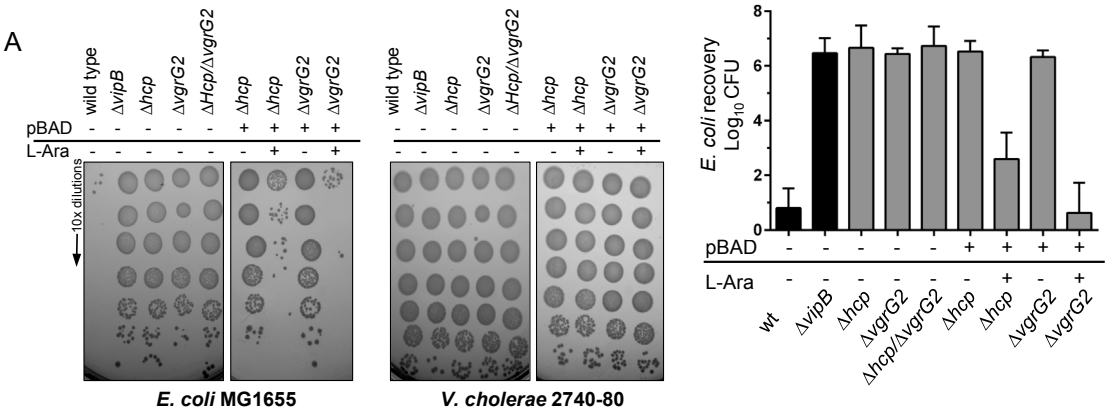

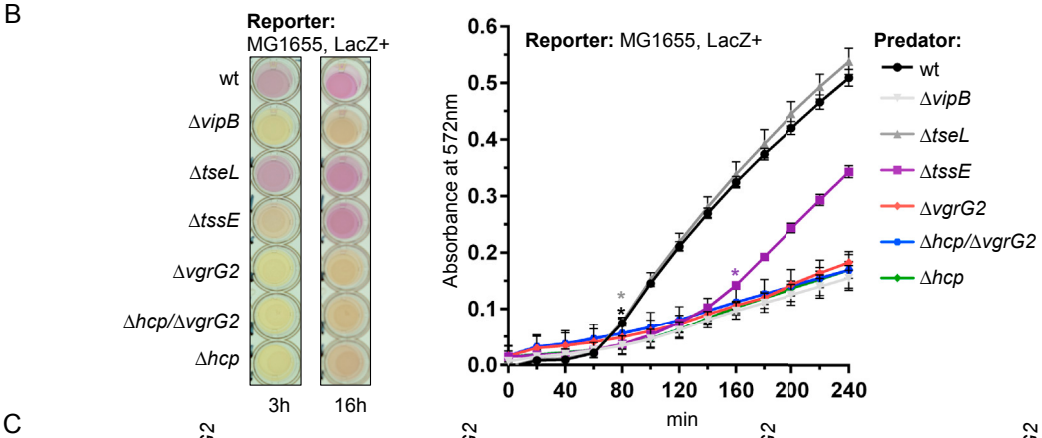

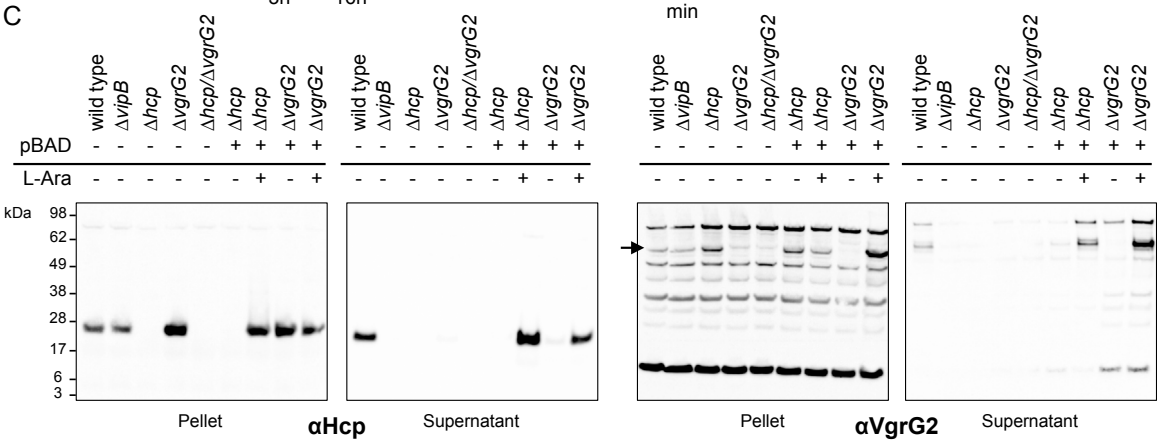

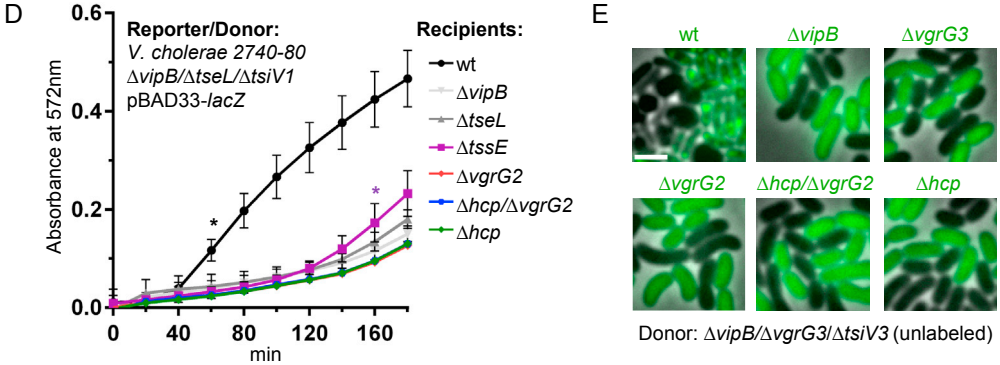

(legend on next page)

Figure S2. The Deletion of *hcp* and *vgrG2* Leads to a Complete Absence of T6SS Activity, Related to Figures 1A and 4

(A) Depicted are recovered cells after 2 hr of co-incubation on LB agar plate. Images represent examples of the quantified data in the graph on the right. Black bars represent positive (wild-type) and negative control (*ΔvipB*). The presence or absence of pBAD vectors and induction of protein expression for complementation is indicated by "+" or "-", respectively.

(B) Indicated *V. cholerae* strains were co-incubated with LacZ+ *E. coli* (reporter). A representative image of a 96-well plate is shown after 180 min and subsequent over-night co-incubation of indicated strains is shown on the left. For cell lysis quantification (right) indicated recipient strains were mixed with the donor strain and incubated for 3 h at 37°C in 96-well plate. Absorbance was measured in 20 min intervals at 572 nm. Colored asterisks mark time point from which chlorophenol red absorbance was significantly higher as compared to background absorbance (*ΔvipB* + reporter) determined by unpaired t-test.

(C) Presence of Hcp (left) and VgrG2 (right) was assessed by western blotting in pellet and cell-free supernatant fractions. Predicted molecular weight for Hcp: 18 kDa; VgrG2: 72 kDa. The presence and absence of pBAD vectors and induction of protein expression for complementation is indicated by "+" or "-", respectively, arrow indicates specific band for VgrG2.

(D) Lipase sensitive, T6SS-, lacZ+ reporter strain was co-incubated with indicated recipient strains at a ratio of 1:10 (reporter/recipient) for the detection of reporter cell lysis. Bacterial mixtures were incubated for 3 h at 37°C in 96-well plate. Absorbance was measured in 20 min intervals at 572 nm. Colored asterisks mark time point from which chlorophenol red absorbance was significantly higher as compared to background absorbance (*ΔvipB* + reporter) determined by unpaired t-test.

(E) A VgrG3 sensitive, T6SS- reporter strain was used as donor for interbacterial protein complementation. Bacterial mixtures were co-incubated on LB agarose pad under a glass cover slip for 1 h prior to screening for cell-rounding. Representative images of cells are shown and are a merge of phase contrast and GFP fluorescence channels depicting cell-rounding in VgrG3 sensitive donor cells (black label, no fluorescence) and indicated *vipA-msfGFP* background strains (green label, GFP fluorescence). Cell-rounding was assessed in 40'000 donor cells for each mixture. Scale bar = 2 μm.

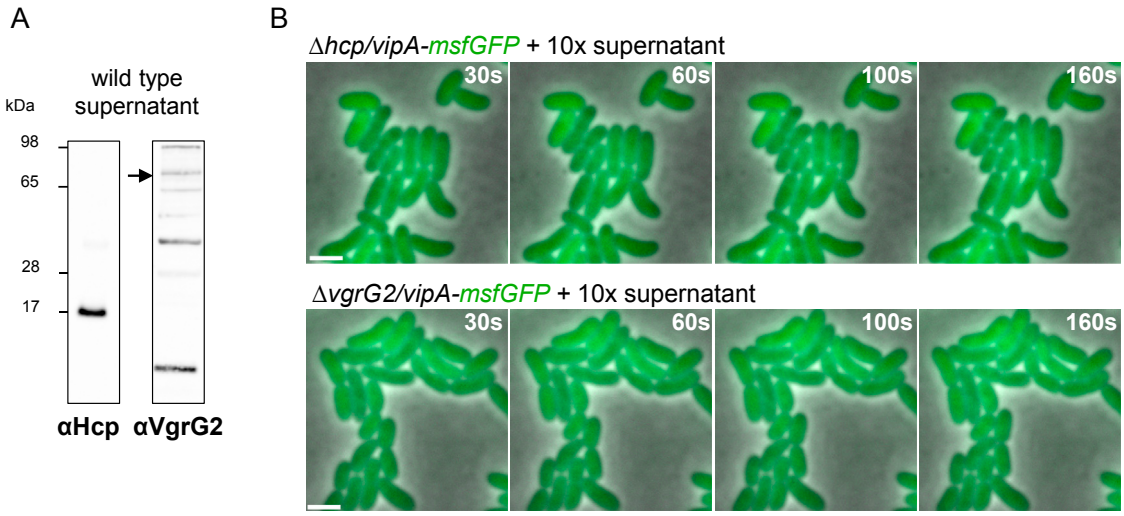

Figure S3. Interbacterial Protein Complementation Relies on T6SS-Mediated Protein Translocation into Recipient Cells, Related to Figure 1

(A) Supernatant from a fresh day culture of wild-type *V. cholerae* 2740-80 was concentrated 10-fold by Amicon spin tube according to the manufacturer's recommendations. Presence of Hcp and VgrG2 (indicated by arrow) was confirmed by western blot on diluted (1x) precipitated supernatant.

(B) Indicated strains were prepared for imaging as normal but resuspended in 10x concentrated supernatant. Depicted are individual frames from a 5 min time-lapse movie and are a merge of phase contrast and GFP fluorescence channel. No T6SS activity was detected during 2 hr observation period. Scale bars = 2 μm.

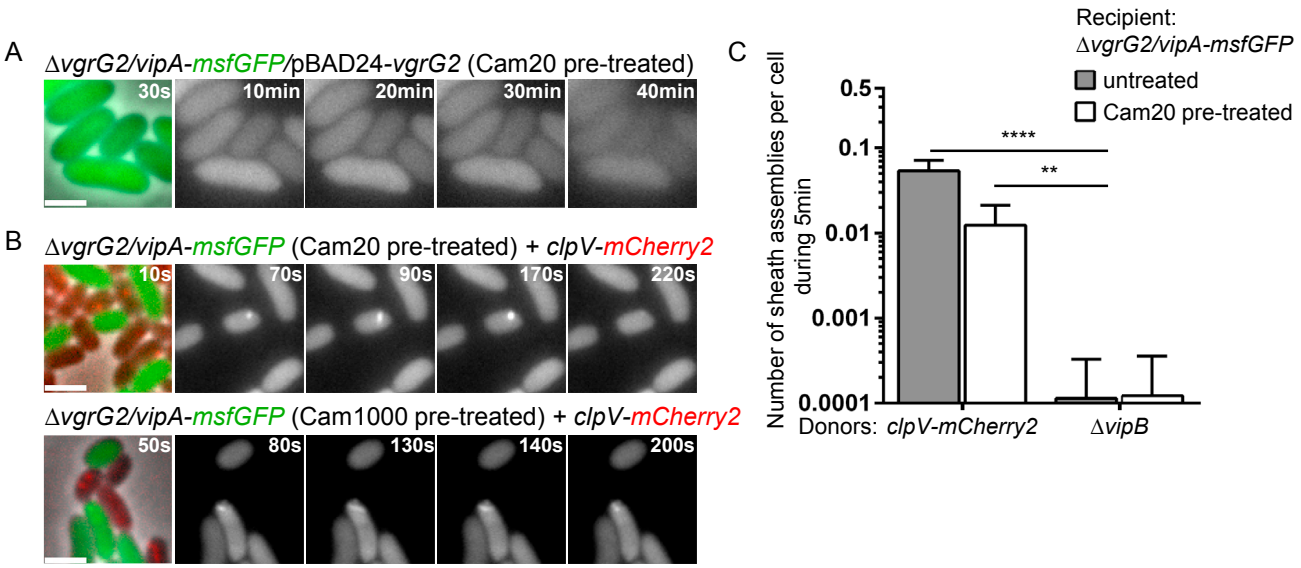

Figure S4. Interbacterial Protein Complementation Does Not Require De Novo Protein Synthesis for the Initiation of a New T6SS Assembly, Related to Figure 1

(A) VgrG2 was expressed from pBAD24 vector in *vipA-msfGFP* strains lacking *vgrG2*. Thirty minutes prior to imaging 20 μg/ml chloramphenicol was added to the cultures. Subsequently cells were spotted on a pad with 0.1% L-arabinose. The time after protein induction is indicated. Depicted are individual frames of a 60 min time-lapse movie. The first frame shows all cells and is a merge of phase contrast and GFP fluorescence channels, whereas the following 4 frames show only GFP fluorescence channel to clearly visualize sheath assembly. No sheath assembly was detected within 1 hr of imaging.

(B) *VipA-msfGFP* labeled strains lacking *vgrG2* were pretreated with chloramphenicol (20 μg/ml for 30 min – top; 1 mg/ml for 90 min – bottom) prior to mixing them with untreated donor cells for interbacterial protein complementation assay. Depicted are individual frames of a 5 min time-lapse. The first frame shows all cells and is a merge of phase contrast, GFP (chloramphenicol treated *ΔvgrG2* - T6SS- recipient) and mCherry2 (wild-type donor) fluorescence channels. The following four frames only show GFP fluorescence channel to visualize sheath dynamics. Scale bar = 2 μm.

(C) Sheath assembly was monitored in untreated and chloramphenicol pretreated (20 μg/ml for 30min) *ΔvgrG2/vipA-msfGFP* strains for 5 min immediately after co-incubation either with *clpV-mCherry2* (wild-type T6SS activity) or *ΔvipB* (T6SS-) donor cells. Total number of sheath assemblies was counted in 5′000 GFP+ cells for indicated strains. Data are represented as mean ± SD. **** = $p < 0.0001$; ** = $p < 0.01$; one-way ANOVA and Tuckey post hoc test for multiple comparison.

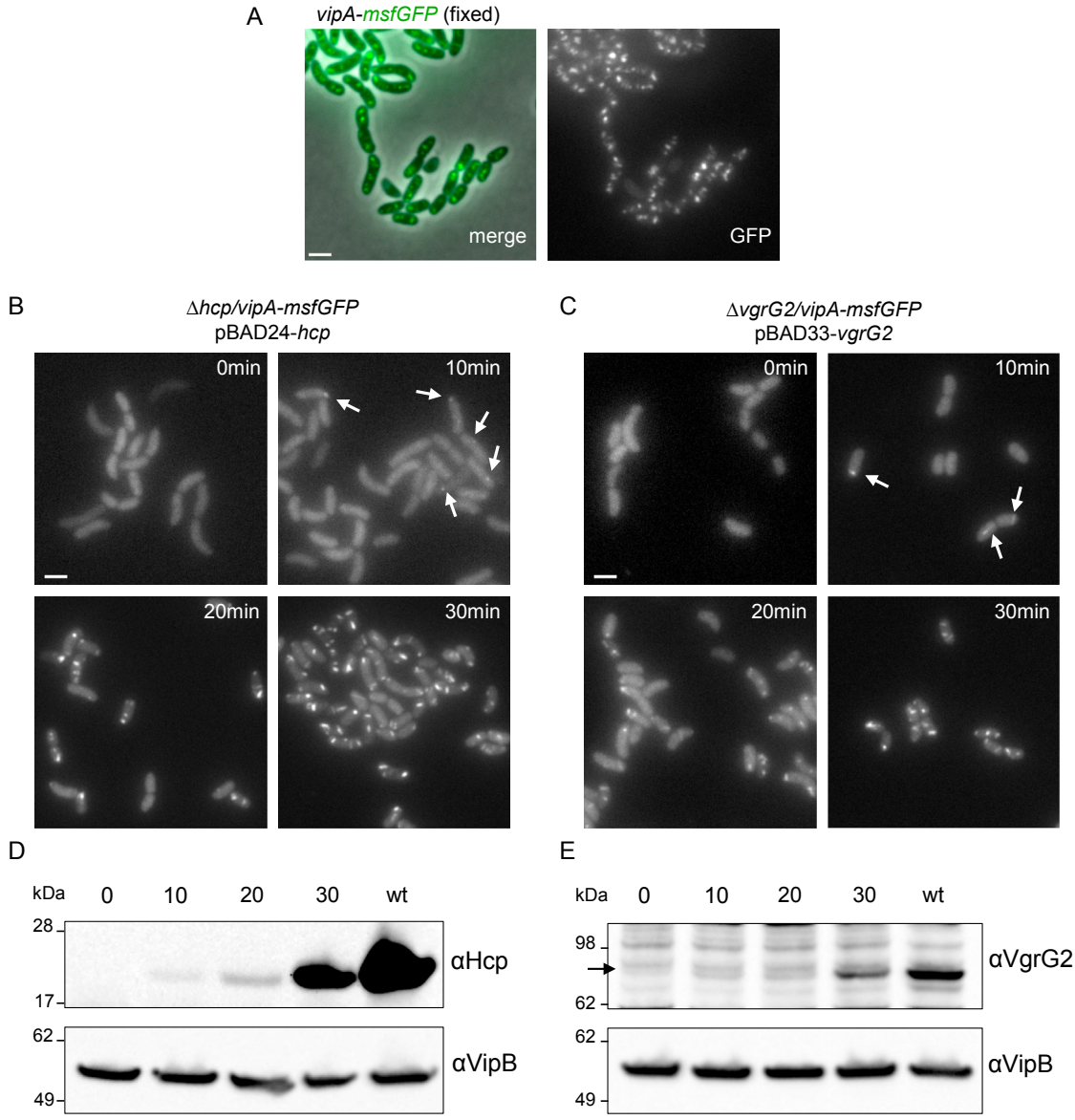

Figure S5. Protein Concentrations of VgrG2 and Hcp Correlate with the Number and Length of Sheath Assemblies, Related to Figure 2

(A) Representative image showing T6SS sheaths in wild-type *vipA-msfGFP* labeled *V. cholerae* strain. Cells were fixed by the direct addition 4% formaldehyde, 0.2% glutaraldehyde to the culture and incubated for 20 min at room temperature. Subsequently fixative was removed and cells were resuspended in PBS and stored until microscopic analysis.

(B and C) Hcp (B) or VgrG2 (C) were expressed from pBAD vectors in *vipA-msfGFP* background strains lacking *vgrG2* or *hcp1/hcp2*, respectively by the addition of 0.01% L-arabinose to the culture. The time after harvesting and fixing (as described above) a sample of to the culture is indicated. Images show representative cells in GFP fluorescence channel to visualize sheath assembly. Arrows indicate first sheath assemblies. Scale bar = 2 μm.

(D and E) Presence of Hcp (D) and VgrG2 (E) was assessed by western blotting in pellet fractions harvested and immediately boiled in SDS sample buffer at indicated time points after the addition of 0.01% L-arabinose and compared to wild-type levels. Arrow indicates specific (lower) band for VgrG2. Presence of VipB was detected and serves as a loading control.

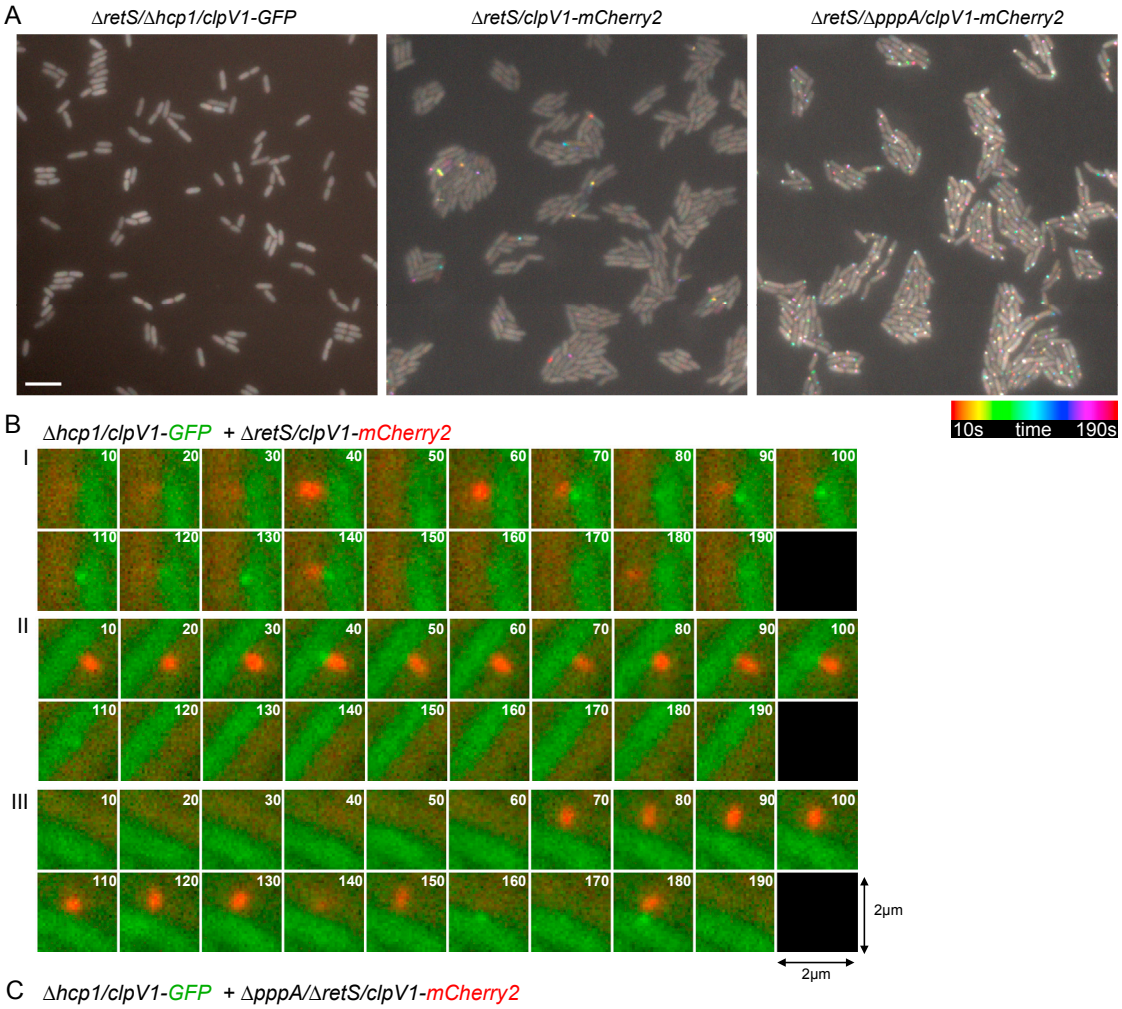

(legend on next page)

Figure S6. *P. aeruginosa* Displays T6SS Activity upon Interbacterial Protein Complementation, Related to Figure 6

(A) Temporal color coded projections of 3 min time-lapse series of ClpV1-GFP or ClpV1-mCherry2 fluorescence signal are depicted for each indicated strain (50 × 50 μm fields). Scale bar is 5 μm. Time-color code is shown.

(B and C) Representative time-lapse series of six of ClpV1 assembly events between *pppA*+ (B) and *pppA*- (C) donor (*ΔretS/clpV1-mCherry2* - T6SS+, red) and recipient (*ΔretS/Δhcp1/clpV1-GFP* - T6SS-, green) cells are depicted. All 19 frames of a 3 min time-lapse series acquired with a frame rate of 10 s are shown. Image series were corrected to reduce effects of photo-bleaching.

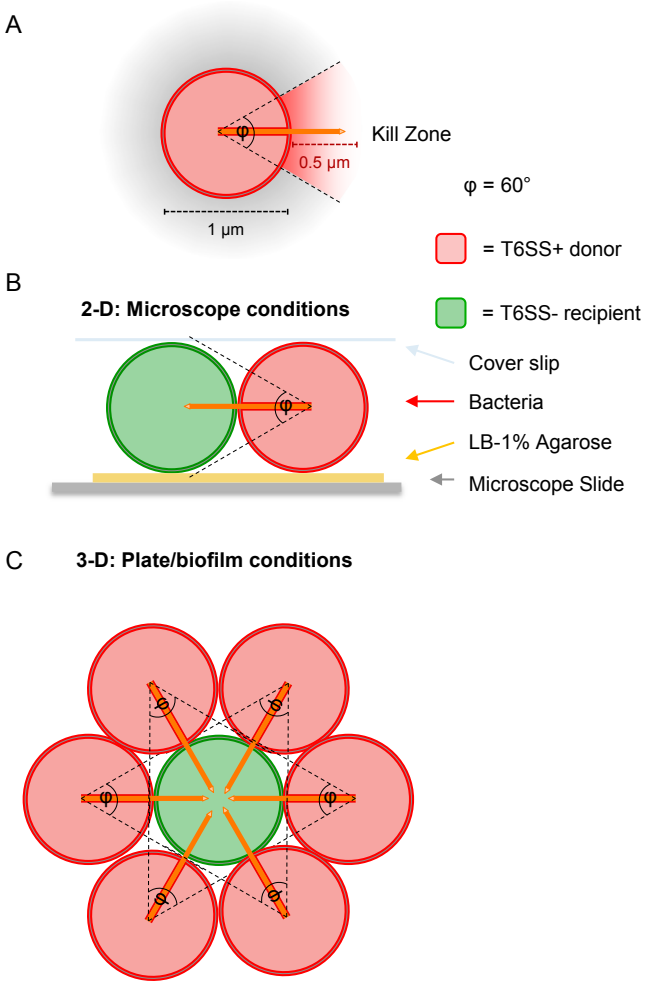

Figure S7. Theoretical Efficiency of T6SS Substrate Delivery, Related to Figure 7

(A) An average fully extended T6SS sheath reaches up to 1 μm in length and contracts to half of its initial length, thereby propelling out the inner Hcp tube and associated effectors to a maximum distance of 0.5 μm. It is reasonable to expect that cells lying within a 60° angle of a contracted sheath will be hit by secreted T6SS substrates (Red shade = potential kill zone).

(B) Since *V. cholerae* was shown to assemble its T6SS machinery at random subcellular localization, a donor has maximum one in six chance of translocating its T6SS substrate into target cells.

(C) Dense three-dimensional biofilms may provide 6 times more contact sites to sister cells than in a single layer of cells. Bacterial cells are simplified as cross-sections.